Cosmic-ray Hadrons at GeV—TeV energies and CALET

Nicholas Cannady

ISCRA 2022

Erice, Italy

Primary vs. secondary nuclei

Some species in the CR flux are overrepresented compared to local Galactic (i.e. Solar System) abundances

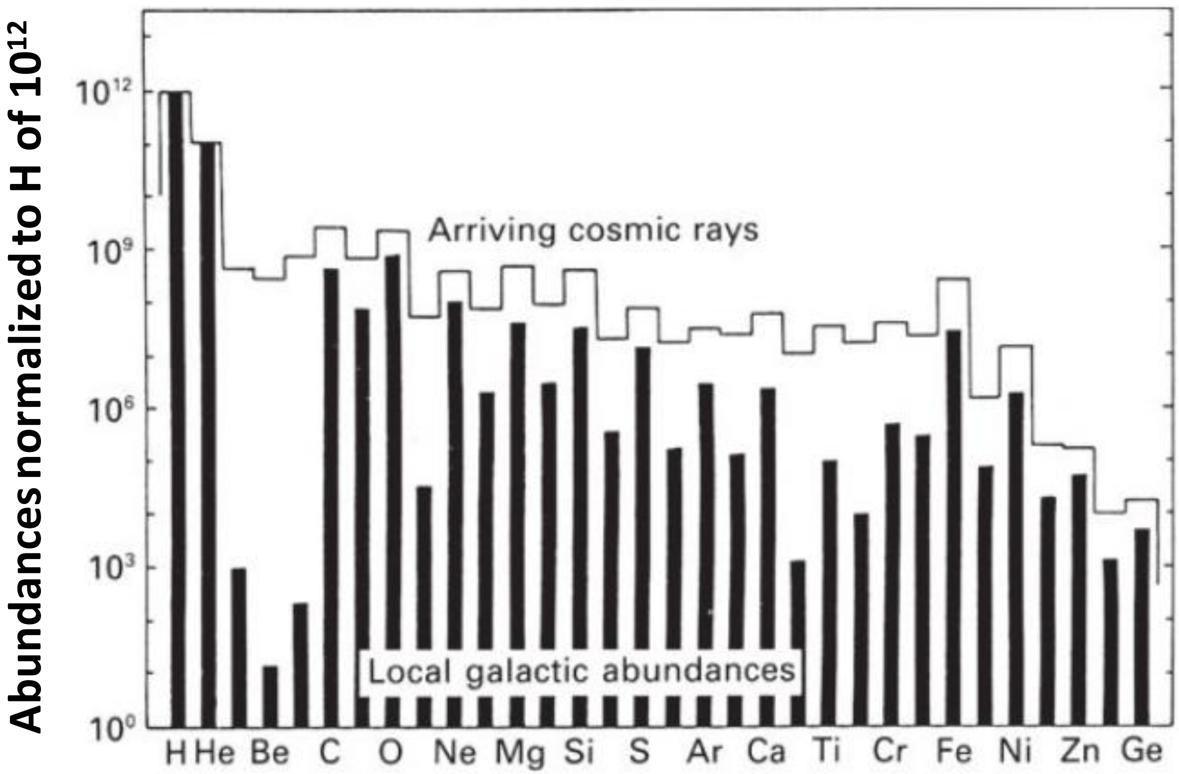

Cycle of matter in the Galaxy

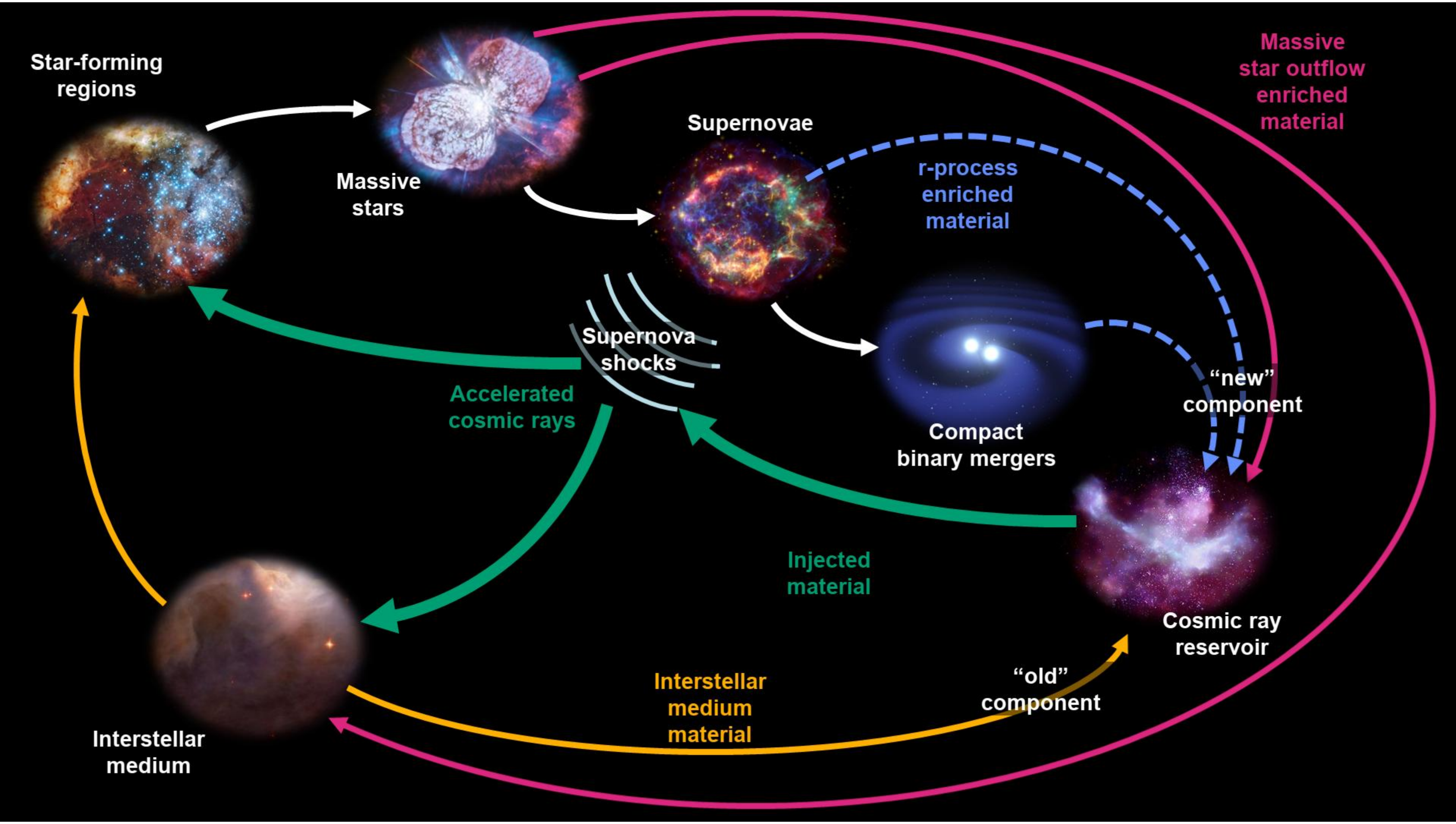

Abundances of cosmic-ray species

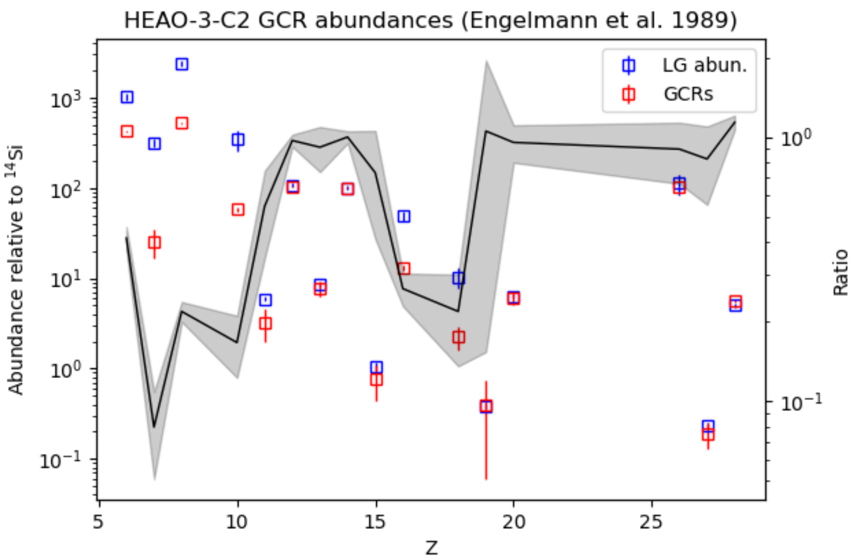

Abundances as measured at Earth

Abundances of cosmic-ray species

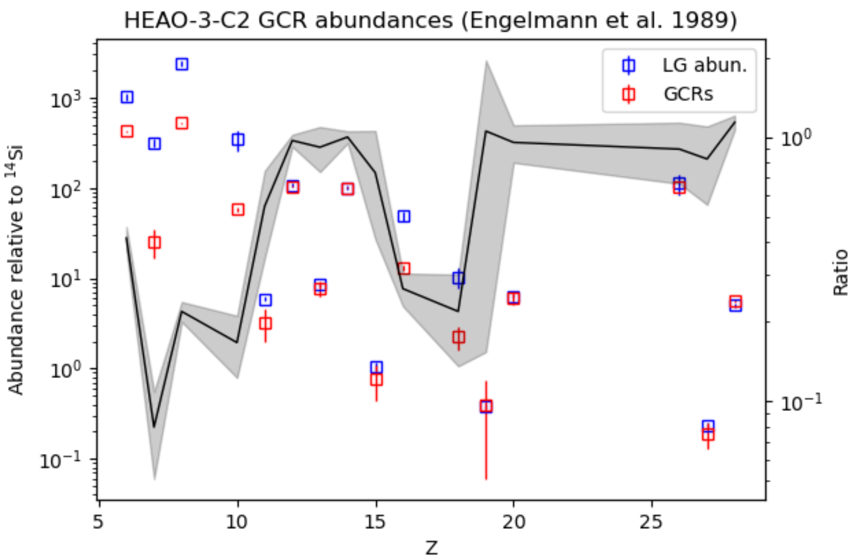

Abundances as measured at Earth

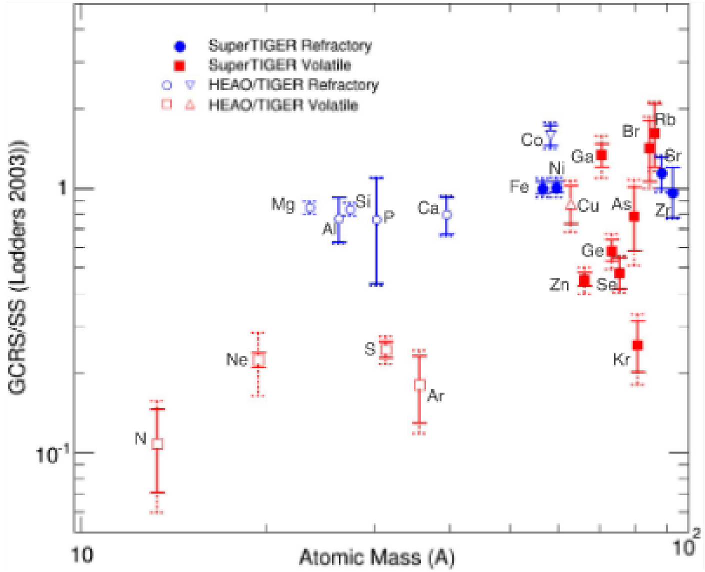

Normalized to Solar System abundances

Abundances of cosmic-ray species

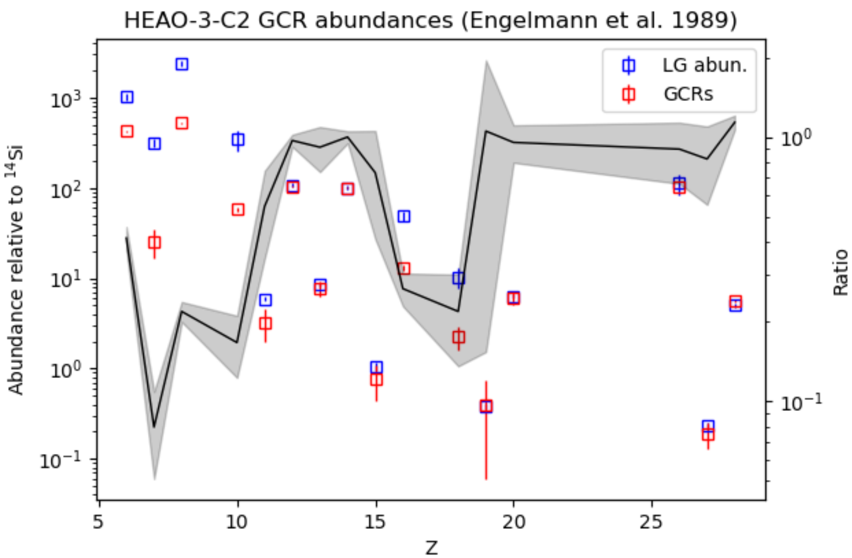

Abundances as measured at Earth

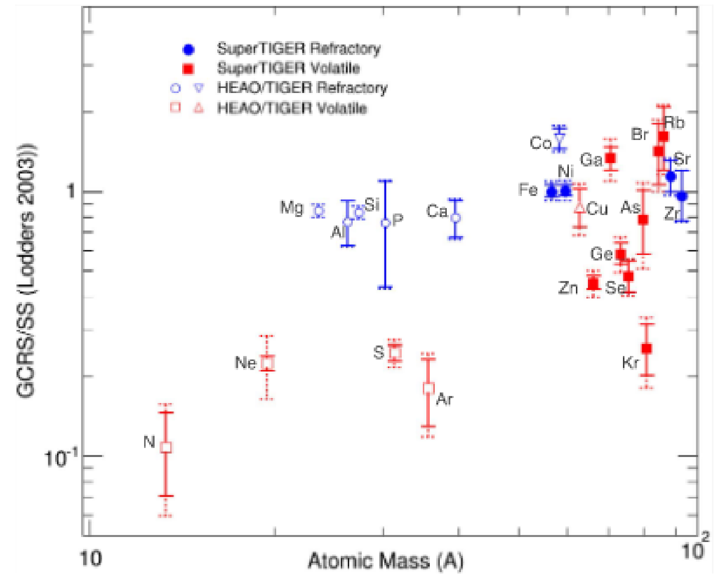

Normalized to Solar System abundances

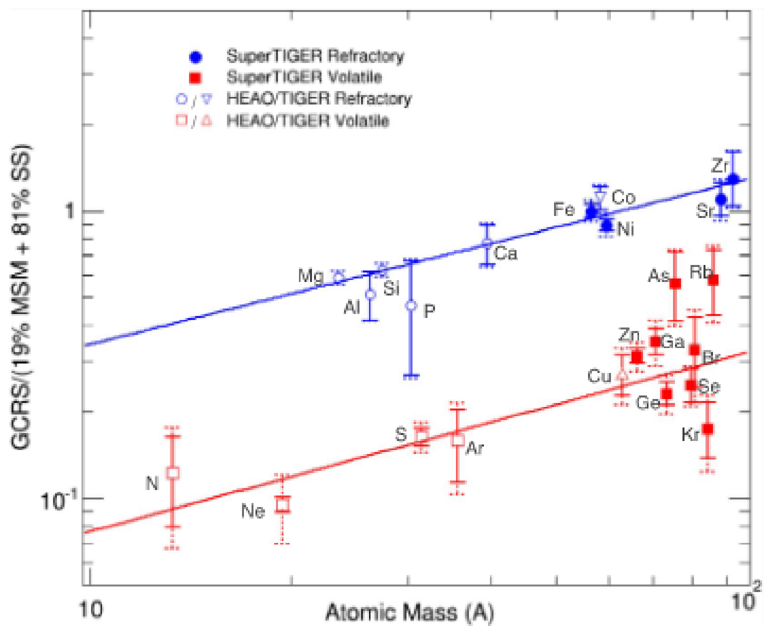

Normalized to 19% massive star material (WR winds and SNe ejecta) and 81% Solar

Plot: Murphy et al. 2016
Incl. HEAO, TIGER, and SuperTIGER measurements

SS: Lodders 2003
MSM: Woosley & Heger 2007

OB Association model of injection

Synthesis of MSM in OB Associations

OB Association model of injection

Synthesis of MSM in OB Associations

Condensation onto grains, along with other nuclei and p

Collection of charge on outside of grains -> increase rigidity for same momentum

e.g. Ivlev et al. 2018

OB Association model of injection

Synthesis of MSM in OB Associations

Condensation onto grains, along with other nuclei and p

Collection of charge on outside of grains -> increase rigidity for same momentum

e.g. Ivlev et al. 2018

Charge sputtering cross section Lingenfelter et al. 2019

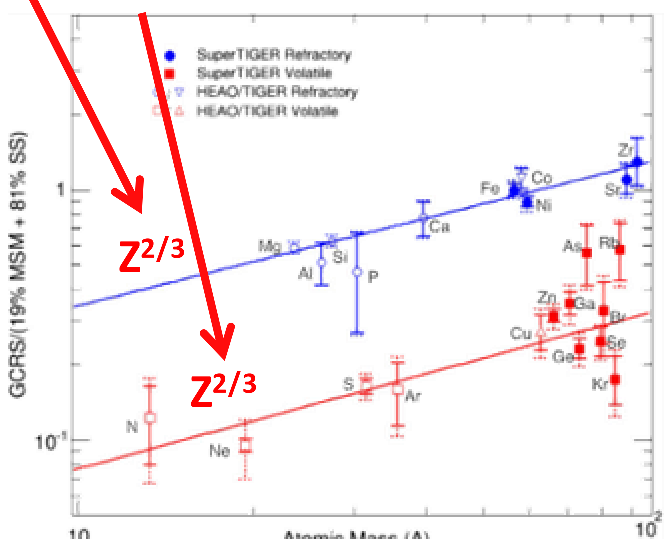

Efficient acceleration of grains to supra-thermal energies

Grains are dissociated through collisions, fragments accelerated to CR energies

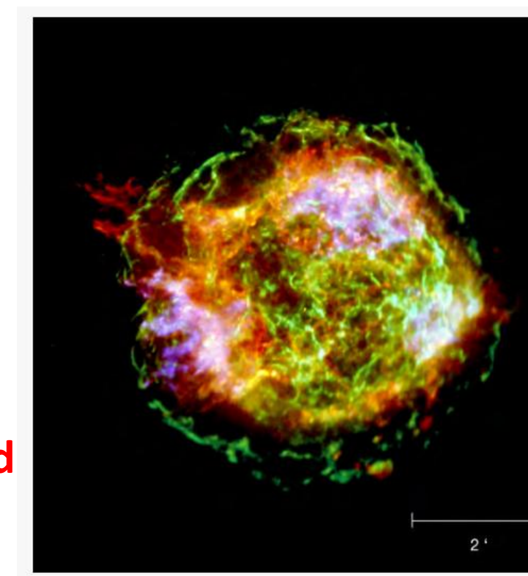

Stages of GCR lifetime

Synthesis:

Stellar fusion processes, massive star ejecta, explosive nucleosynthesis

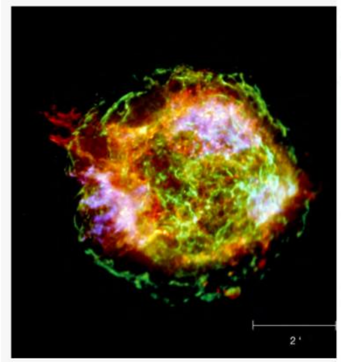

Injection:

Dust grain acceleration to supra-thermal energies in strong shocks

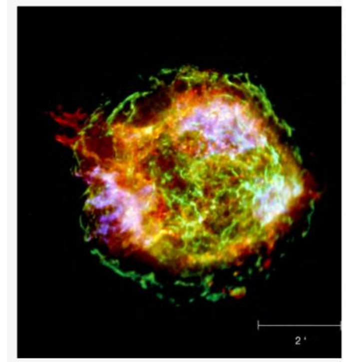

Acceleration:

Grain sputtering and acceleration to GCR energies in strong shocks

Propagation:

Accelerated GCRs escape local environment and transport throughout the Galaxy

Primary vs. secondary nuclei

Some species in the CR flux are overrepresented compared to local Galactic (i.e. Solar System) abundances

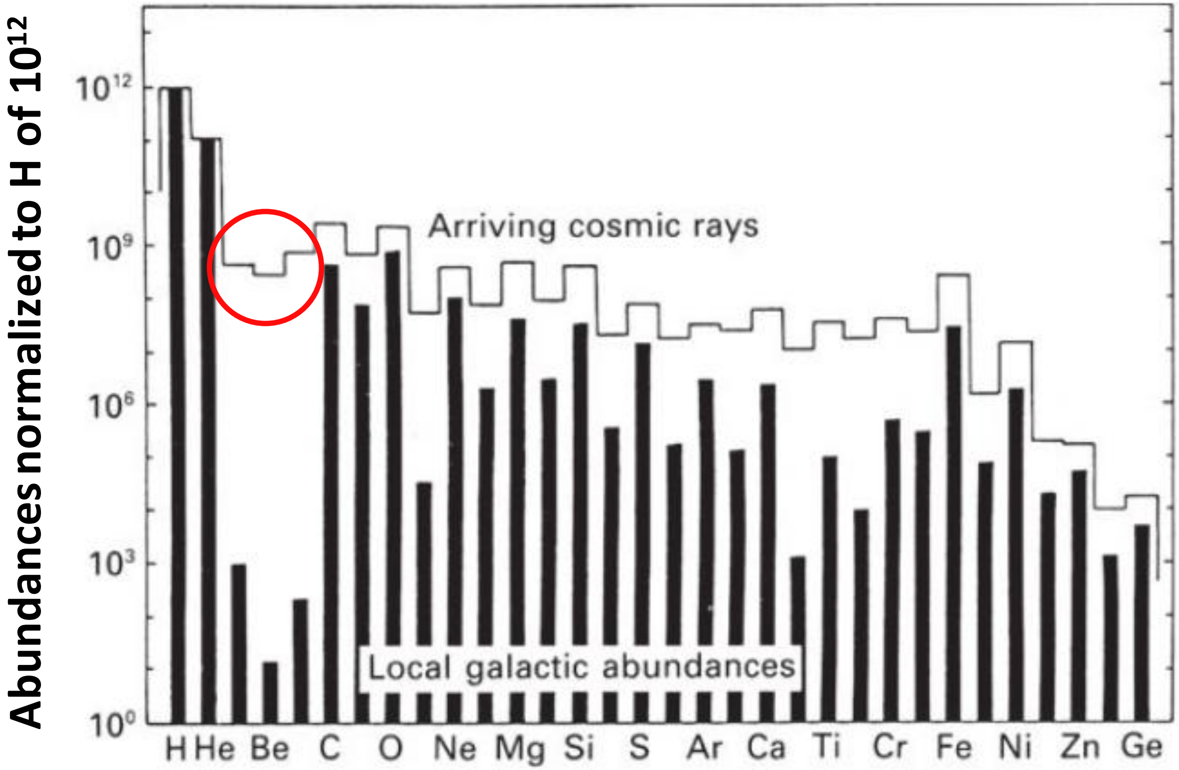

Not due to enrichment of MSM, must arise from fragmentation of heavier nuclei producing significant secondary component

Transport equation for nuclei

For a nuclear species i,

$$\frac{dN_i}{dt} = D\nabla^2 N_i + \frac{\partial}{\partial E}[bN_i] + Q_i \underbrace{- \frac{N_i}{\tau_i}}_{\text{Collisions converting species i to lighter nuclei through spallation}} + \underbrace{\sum_{j>i} \frac{P_{ji}}{\tau_j} N_j}_{\text{Collisions converting heavier species j to species i}}$$

Probability of j -> i in collision

Transport equation for nuclei

For a nuclear species i,

$$\frac{dN_i}{dt} = D\nabla^2 N_i + \frac{\partial}{\partial E}[bN_i] + Q_i - \frac{N_i}{\tau_i} + \sum_{j>i} \frac{P_{ji}}{\tau_j} N_j$$

Let's look at the effect of primary spallation into secondaries:
Neglect diffusion, energy losses, and source injection

Transport equation for nuclei

For a nuclear species i,

$$\frac{dN_i}{dt} = D\nabla^2 N_i + \frac{\partial}{\partial E}[bN_i] + Q_i - \frac{N_i}{\tau_i} + \sum_{j>i} \frac{P_{ji}}{\tau_j} N_j$$

Let's look at the effect of primary spallation into secondaries:
Neglect diffusion, energy losses, and source injection

For a **primary** species P,

$$\frac{dN_P}{dt} = -\frac{N_P}{\tau_P}$$

Assumption: nothing significantly contributing to secondary P

For a **secondary** species S,

$$\frac{dN_S}{dt} = -\frac{N_S}{\tau_S} + \frac{P_{PS}}{\tau_P} N_P$$

Transport equation for nuclei

For a **primary** species P,

$$\frac{dN_P}{dt} = -\frac{N_P}{\tau_P}$$

Assumption: nothing significantly contributing to secondary P

For a **secondary** species S,

$$\frac{dN_S}{dt} = -\frac{N_S}{\tau_S} + \frac{P_{PS}}{\tau_P} N_P$$

t

Change independent variable: $\xi = \rho v$

$$t \to \xi$$

$$\tau_P \to \xi_P$$

$$\tau_S \to \xi_S$$

Transport equation for nuclei

For a **primary** species P,

$$\frac{dN_P}{dt} = -\frac{N_P}{\tau_P}$$

Assumption: nothing significantly contributing to secondary P

For a **secondary** species S,

$$\frac{dN_S}{dt} = -\frac{N_S}{\tau_S} + \frac{P_{PS}}{\tau_P} N_P$$

Change independent variable: $\xi = \rho v$ t

$t \rightarrow \xi$

$\tau_P \rightarrow \xi_P$

$\tau_S \rightarrow \xi_S$

$$\frac{dN_P}{d\xi} = -\frac{N_P}{\xi_P} \qquad N_P(\xi) = N_{P0} e^{-\xi/\xi_P} \qquad (N_P(0) = N_{P0})$$

Transport equation for nuclei

For a **primary** species P,

$$\frac{dN_P}{dt} = -\frac{N_P}{\tau_P}$$

Assumption: nothing significantly contributing to secondary P

For a **secondary** species S,

$$\frac{dN_S}{dt} = -\frac{N_S}{\tau_S} + \frac{P_{PS}}{\tau_P} N_P$$

t

Change independent variable: $\xi = \rho v$

$t \rightarrow \xi$

$\tau_P \rightarrow \xi_P$

$\tau_S \rightarrow \xi_S$

$$\frac{dN_P}{d\xi} = -\frac{N_P}{\xi_P} \qquad N_P(\xi) = N_{P0} e^{-\xi/\xi_P} \qquad (N_P(0) = N_{P0})$$

$$\frac{dN_S}{d\xi} = -\frac{N_S}{\xi_S} + \frac{P_{PS}}{\xi_P} N_P \qquad N_S(\xi) = \frac{P_{PS} N_{P0} \xi_S}{\xi_S - \xi_P} e^{-\xi/\xi_P} \left[\mathrm{ex}^{\mathrm{p}} \left(\frac{\xi}{\xi_P} - \frac{\xi}{\xi_S} \right) - 1 \right] \qquad (N_S(0) = 0)$$

Transport equation for nuclei

For a **primary** species P,

$$\frac{dN_P}{dt} = -\frac{N_P}{\tau_P}$$

Assumption: nothing significantly contributing to secondary P

For a **secondary** species S,

$$\frac{dN_S}{dt} = -\frac{N_S}{\tau_S} + \frac{P_{PS}}{\tau_P} N_P$$

Change independent variable: $\xi = \rho v t$

$t \rightarrow \xi$

$\tau_P \rightarrow \xi_P$

$\tau_S \rightarrow \xi_S$

$$\frac{dN_P}{d\xi} = -\frac{N_P}{\xi_P} \qquad N_P(\xi) = N_{P0} e^{-\xi/\xi_P} \qquad (N_P(0) = N_{P0})$$

$$\frac{dN_S}{d\xi} = -\frac{N_S}{\xi_S} + \frac{P_{PS}}{\xi_P} N_P \qquad N_S(\xi) = \frac{P_{PS} N_{P0} \xi_S}{\xi_S - \xi_P} e^{-\xi/\xi_P} \left[\exp\left(\frac{\xi}{\xi_P} - \frac{\xi}{\xi_S}\right) - 1\right] \qquad (N_S(0) = 0)$$

$$\frac{N_S}{N_P} = \frac{P_{PS} \xi_S}{\xi_S - \xi_P} \left[\exp\left(\frac{\xi}{\xi_P} - \frac{\xi}{\xi_S}\right) - 1\right]$$

Secondary-to-primary ratio for light nuclei

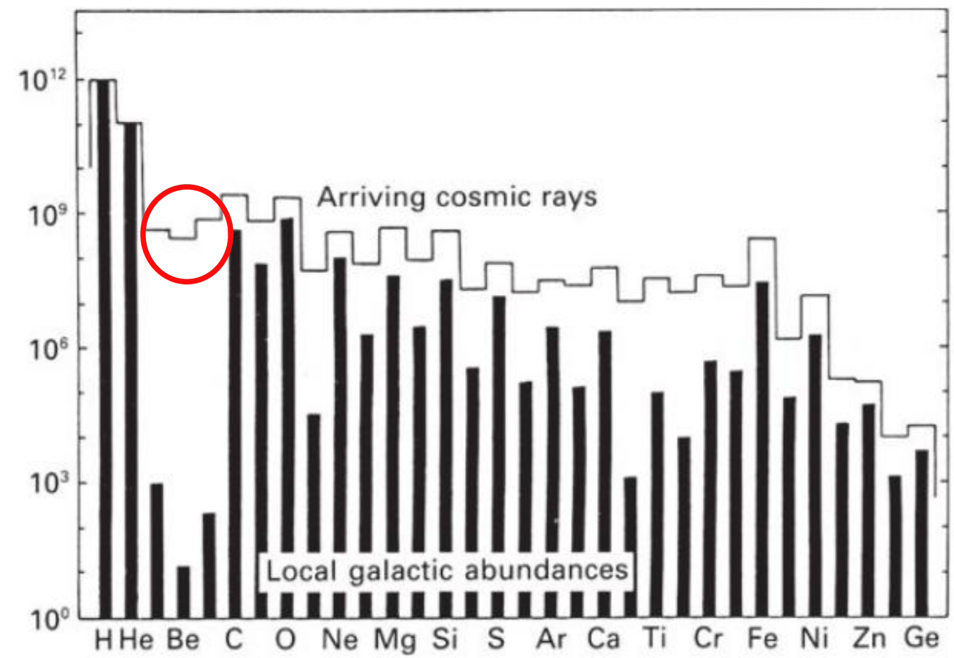

Observed abundance ratio of LiBeB / CNO ~ 0.25

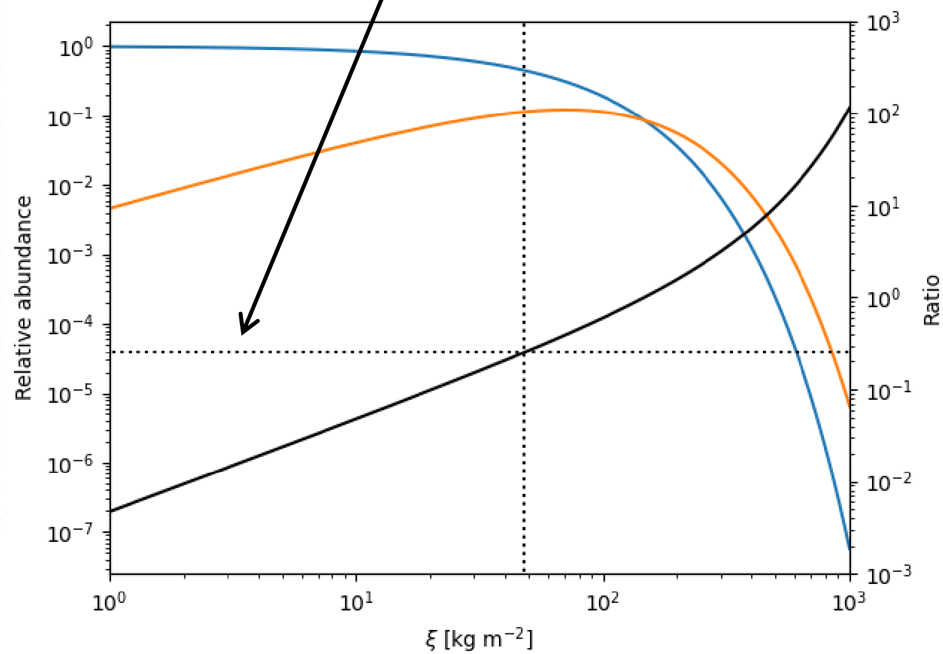

$0 \quad \rho \approx 1\, H\, atom/cm^3$

$\sigma_P \approx 280\ mb$

$\sigma_S \approx 20\ mb$

$P_{PS} \approx 0.28$

$\longrightarrow$

$\xi_P \approx 60\ kg\ m^{-2}$

$\xi_S \approx 84\ kg\ m^{-2}$

Corresponds to grammage passed through of $\xi \approx 48\ kg\ m^{-2}$ or ~100s kpc distance scales

Secondary-to-primary ratio for light nuclei

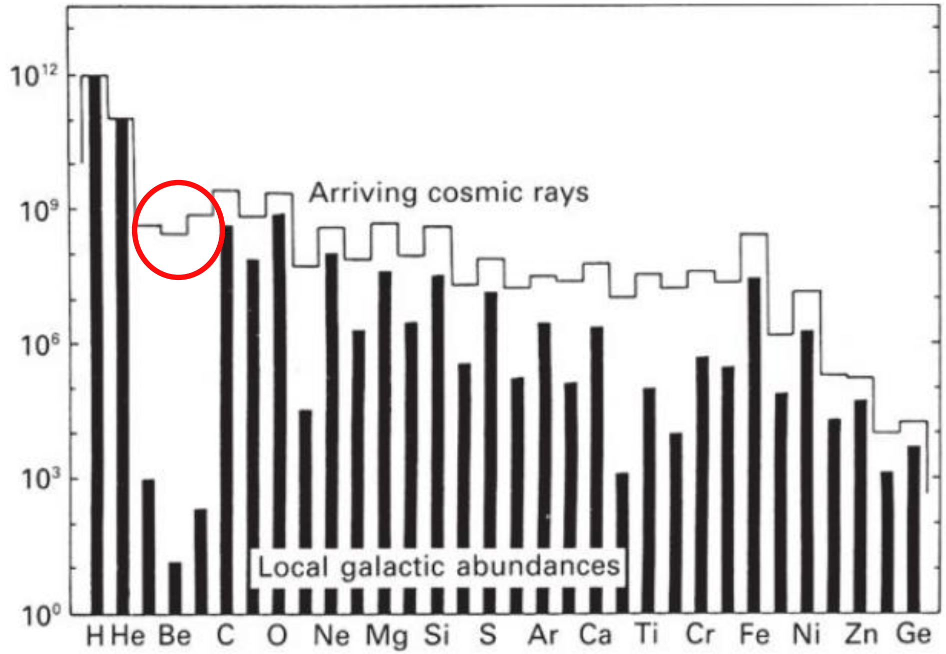

Observed abundance ratio of LiBeB / CNO ~ 0.25

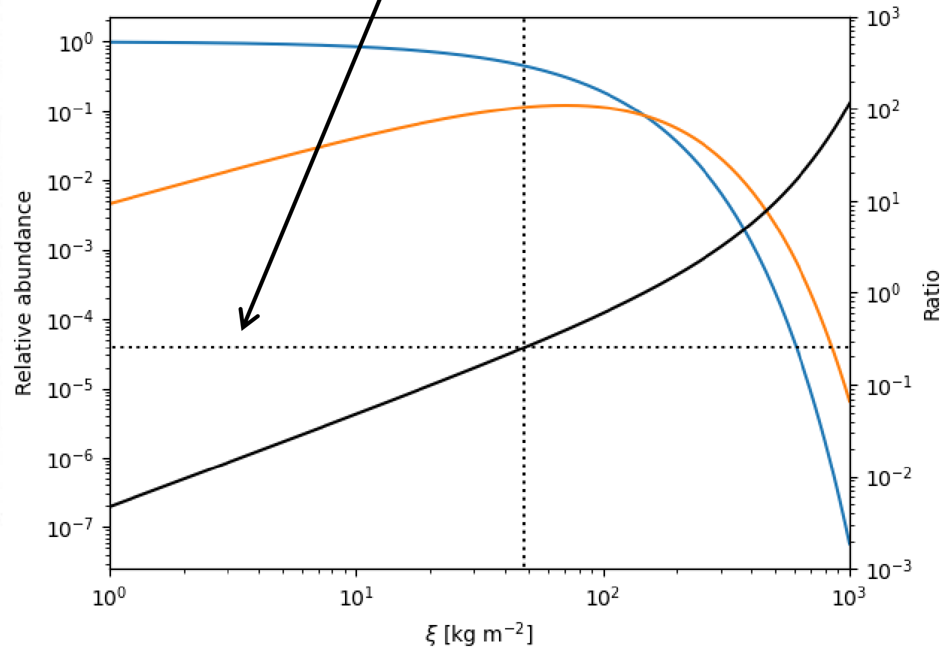

$0 \quad \rho \approx 1\ H\ atom/cm^3$

$\sigma_P \approx 280\ mb$

$\sigma_S \approx 200\ mb$

$P_{PS} \approx 0.28$

$\longrightarrow$

$\xi_P \approx 60\ kg\ m^{-2}$

$\xi_S \approx 84\ kg\ m^{-2}$

Corresponds to grammage passed through of $\xi \approx 48\ kg\ m^{-2}$ or ~100s kpc distance scales

More realistic results require (at least) reintroduction of the diffusion term to account for distribution of path lengths traveled by particles (rather than assuming the average)

Secondary-to-primary ratios

Beyond this small illustrative example, the real situation is much more complex:

- Diffusion, energy loss, and source terms that we neglected
  - Treatment of diffusion leads to different distributions of pathlengths which modify the resulting secondary/primary ratios
    - Isotropic diffusion – Gaussian distribution of pathlengths
    - Leaky box model – exponential distribution of pathlengths
- Energy dependence of parameters in the transport equation
  - Diffusion coefficient
  - Energy loss and source injection terms
- Varying levels of “primary-ness” for each species measured separately
  - Mostly pure primaries, e.g. p, He, C, O, …, Si, …, Fe
  - Mixed, e.g. N with significant primary component and secondary component from interactions of primary O
  - Mostly pure secondaries, e.g. Li, Be, B

Secondary-to-primary ratios

Beyond this small illustrative example, the real situation is much more complex:

- Diffusion, energy loss, and source terms that we neglected
  - Treatment of diffusion leads to different distributions of pathlengths which modify the resulting secondary/primary ratios
    - Isotropic diffusion – Gaussian distribution of pathlengths
    - Leaky box model – exponential distribution of pathlengths
- Energy dependence of parameters in the transport equation
  - Diffusion coefficient
  - Energy loss and source injection terms
- Varying levels of "primary-ness" for each species measured separately
  - Mostly pure primaries, e.g. p, He, C, O, …, Si, …, Fe
  - Mixed, e.g. N with significant primary component and secondary component from interactions of primary O
  - Mostly pure secondaries, e.g. Li, Be, B

Energy-dependent measurement of elemental CR spectra up to the limits of Galactic accelerators are critical input for models of acceleration and propagation of GCRs

Cosmic-ray all-particle spectrum

Relatively featureless except for small changes in spectral index

Direct measurements are limited to ~several PeV total energies simply by feasibility of required detector size

Only up to the knee, where the transition to extragalactic sources dominating the flux begins

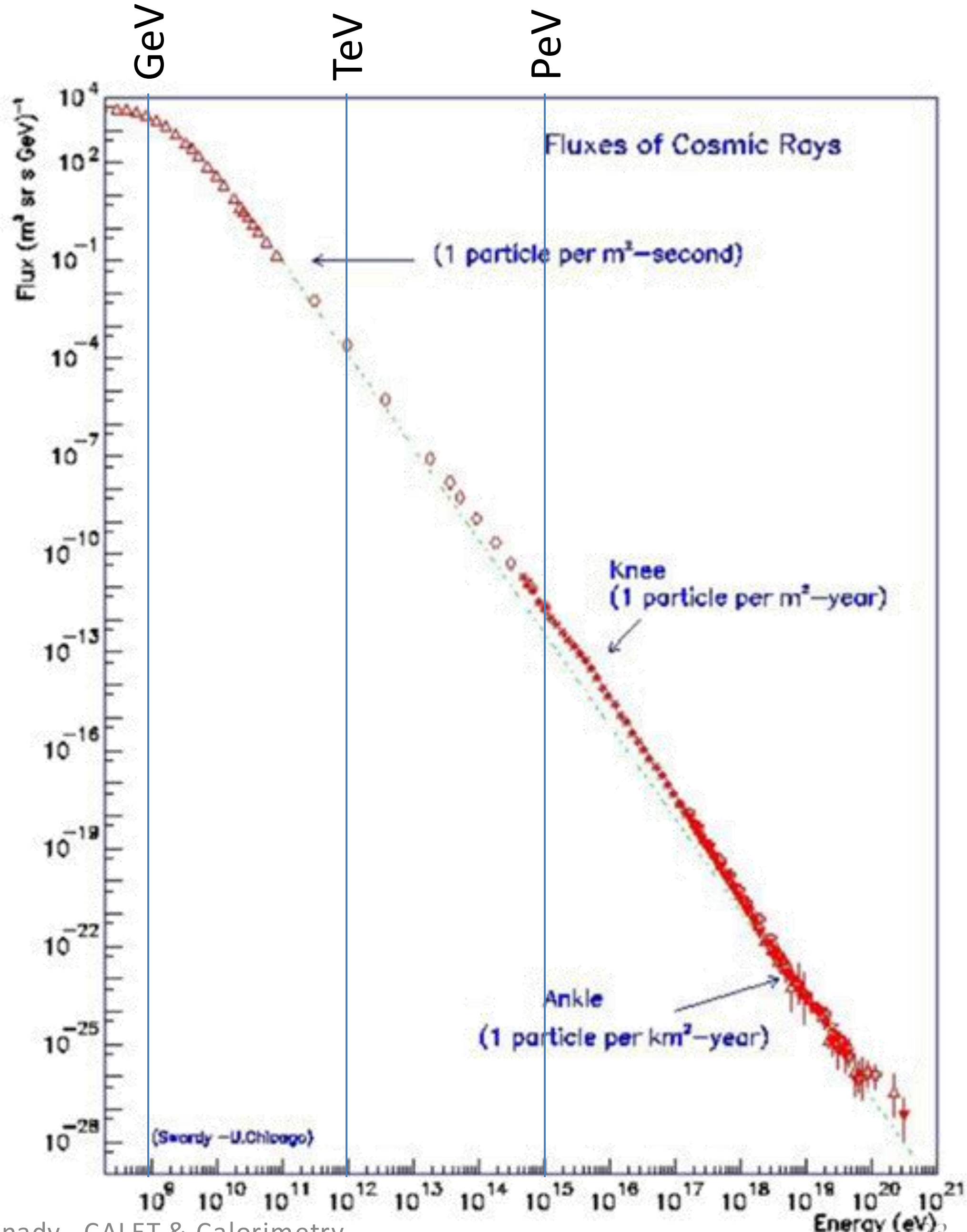

Cosmic-ray all-particle spectrum

Relatively featureless except for small changes in spectral index

Direct measurements are limited to ~several PeV total energies simply by feasibility of required detector size

Only up to the knee, where the transition to extragalactic sources dominating the flux begins

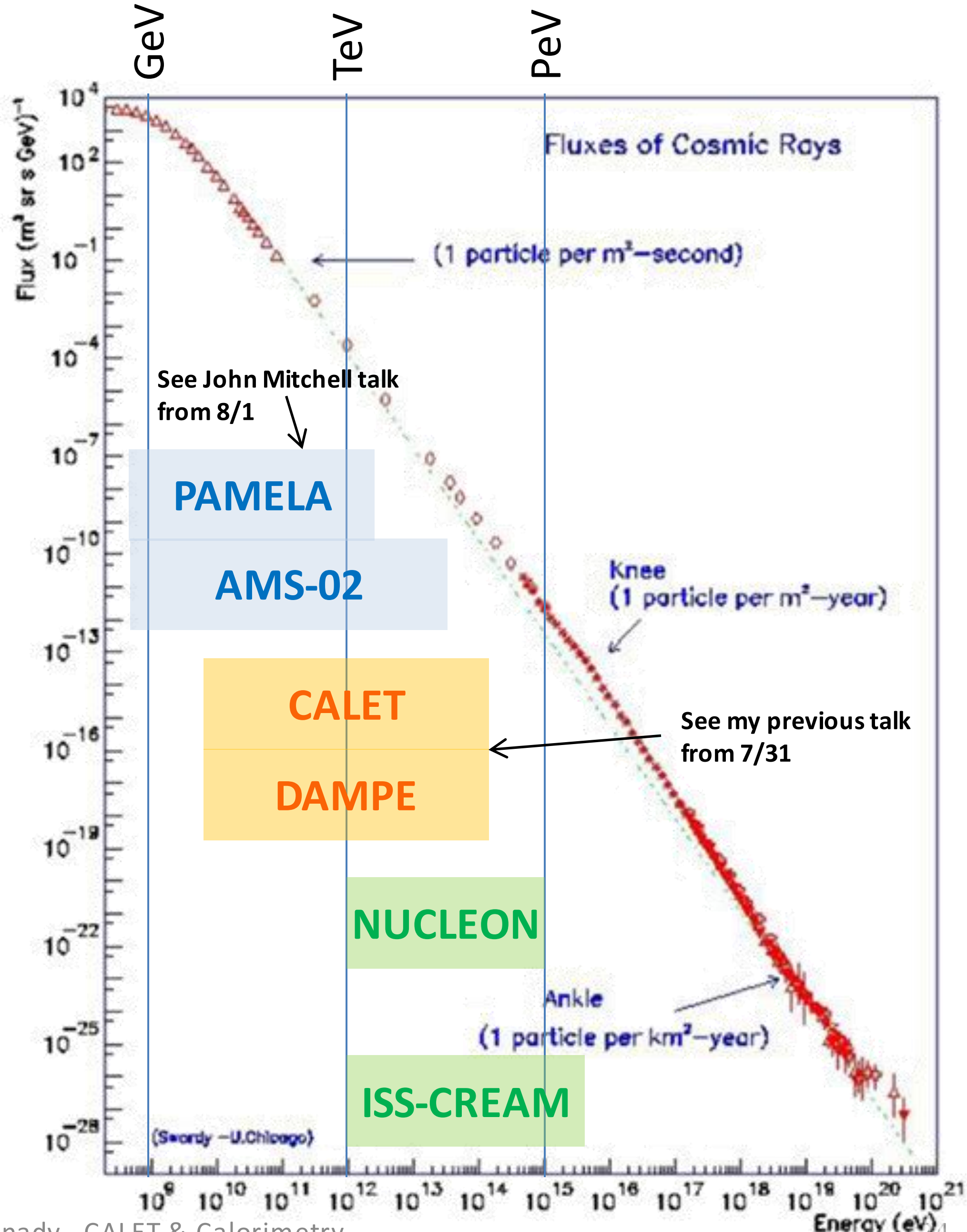

CALET and DAMPE Calorimeters

CALET

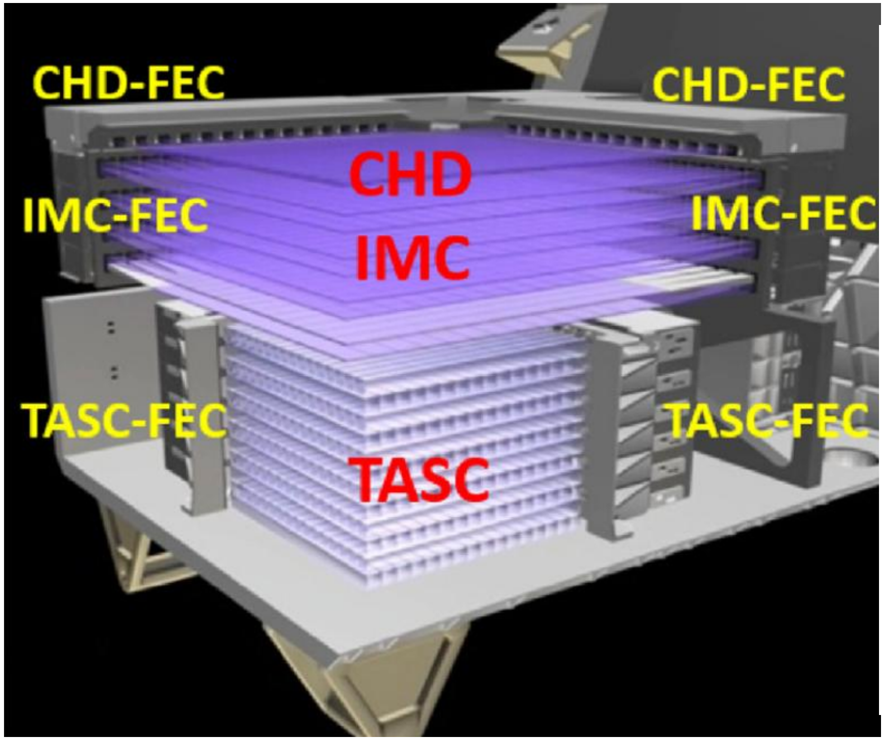

Depth(EM) = 30 X_0

Depth(HAD) = 1.2 λ_p

Geom. Fact. = 0.12 m^2 sr

DAMPE

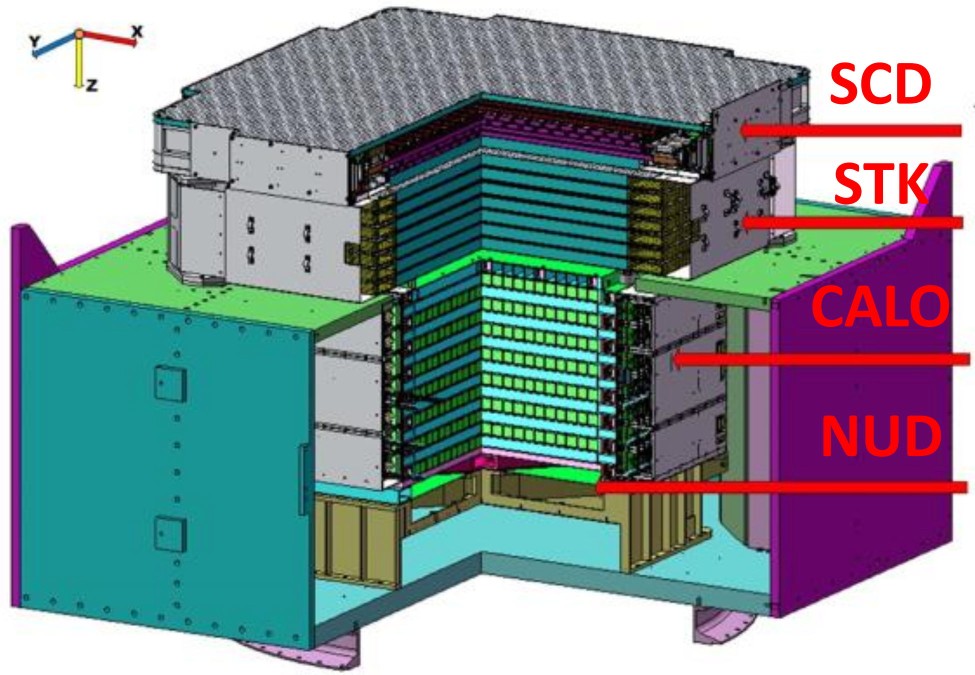

Depth(EM) = 32 X_0

Depth(HAD) = 1.6 λ_p

Geom. Fact. = 0.3 m^2 sr

PAMELA and AMS-02 Spectrometers

PAMELA

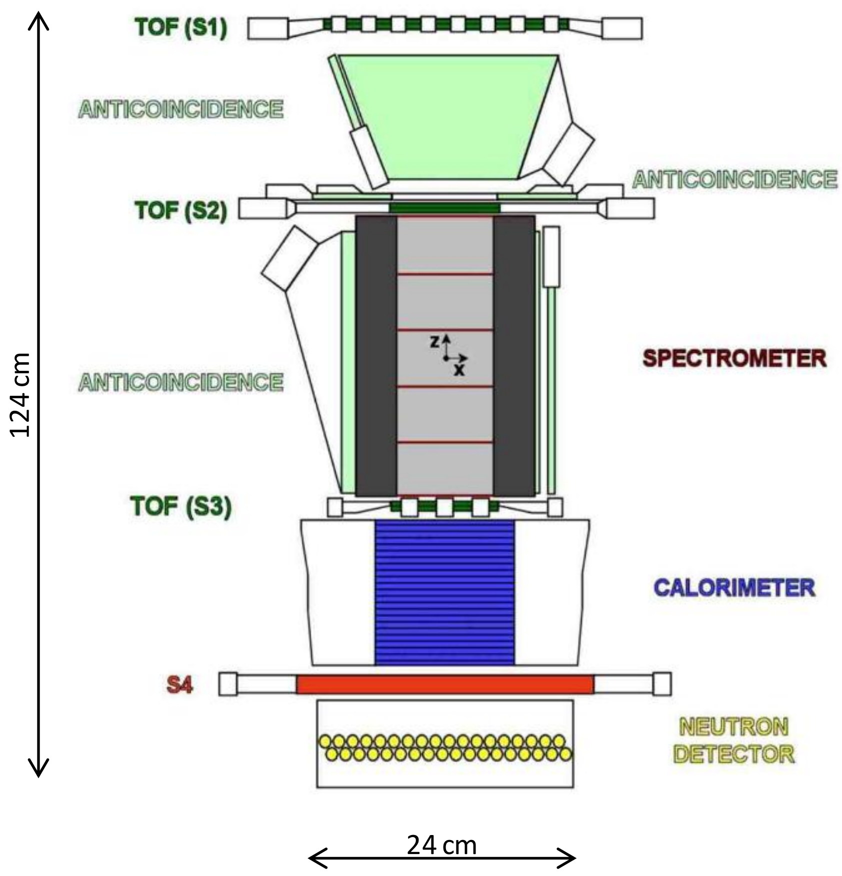

AMS-02

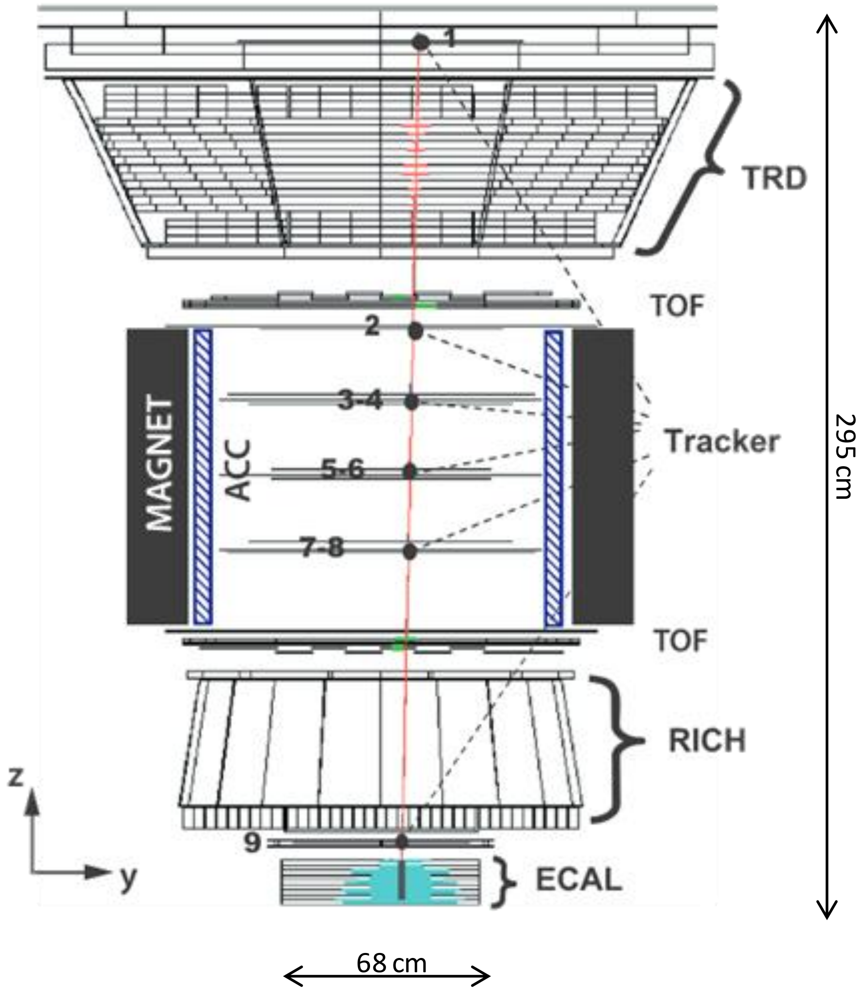

MDR = 740 GV

Acc. = 21.5 cm² sr

MDR = ~3 TV

Acc. = 5000 cm² sr

ATIC and CREAM balloon-borne calorimeters

ATIC

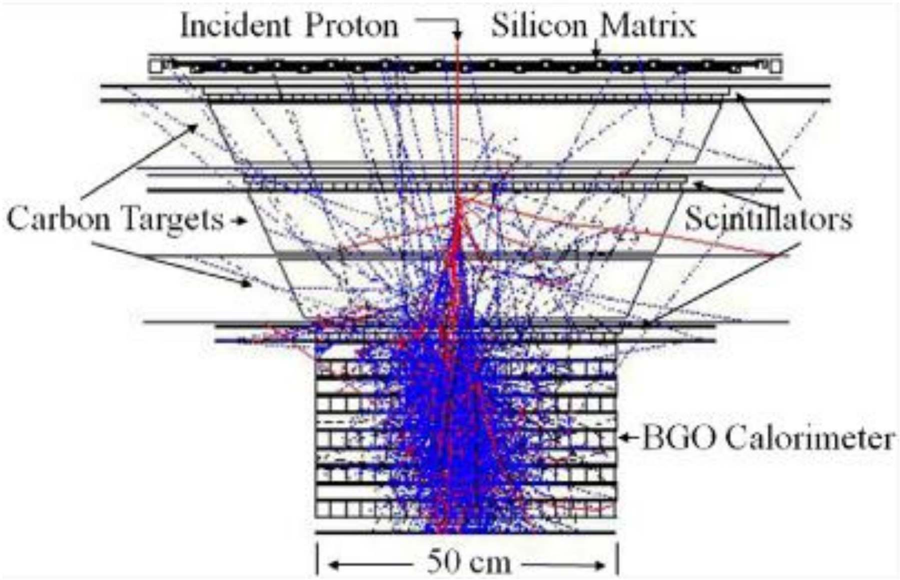

CREAM

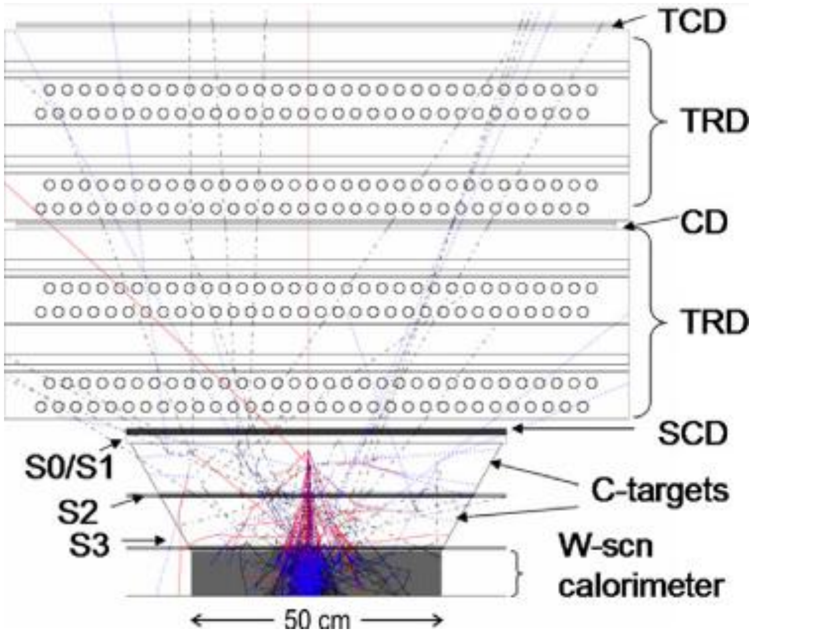

Instrument	Energy measurement technique	Charge range and resolution	Flight duration	Atmospheric depth[a] (g/cm^2)	Effective exposure (m^2-sr-days)	Observed number of protons >6 TeV
ATIC	Calorimeter (0.75 λ_I, 18 X_0)	$1 \leqslant Z \leqslant 28$ $\Delta Z = 0.3$	~48 days	4.3 (7.9)	5	~720
TRACER[a]	TRD	$8 \leqslant Z \leqslant 28$ $\Delta Z = 0.3$ (O) 0.5 (Fe) $3 < Z \leqslant 28$ $\Delta Z = 0.3$ (O) 0.5 (Fe)	~10 days ~4 days	3.9 (9.2)	50 20	None
CREAM	Calorimeter (0.5 λ_I, 20 X_0)	$1 \leqslant Z \leqslant 28$ $\Delta Z = 0.2$	~160 days	3.9 (6.8)	48	>5000
	TRD	$3 < Z \leqslant 28$ $\Delta Z = 0.2$	~42 days	3.9(7.9)	55	None
JACEE	Emulsion (~0.05 λ_I, ~4 X_0)	$1 \leqslant Z \leqslant 28$ Charge group	~60 days (1436 m^2 hr)	5.3 (28)	~10 (644 m^2 hr)	656
RUNJOB	Emulsion (~0.2 λ_I, ~4 X_0)	$1 \leqslant Z \leqslant 28$ Charge group	~60 days (575 m^2 hr)	10 (48)	6 (p); 24 (>C)	Close to JACEE

ISS-CREAM

Space-borne successor to balloon-borne CREAM family of missions

- **Silicon charge detector**
- **Carbon targets induce nuclear interactions**
- **Top and bottom counting detectors for e/p separation**
- **Scintillating fiber – tungsten sheet sampling calorimeter for energy measurement**
- **Boronated scintillator detector for more e/p separation**

Began operations August 2017
Stopped February 2019

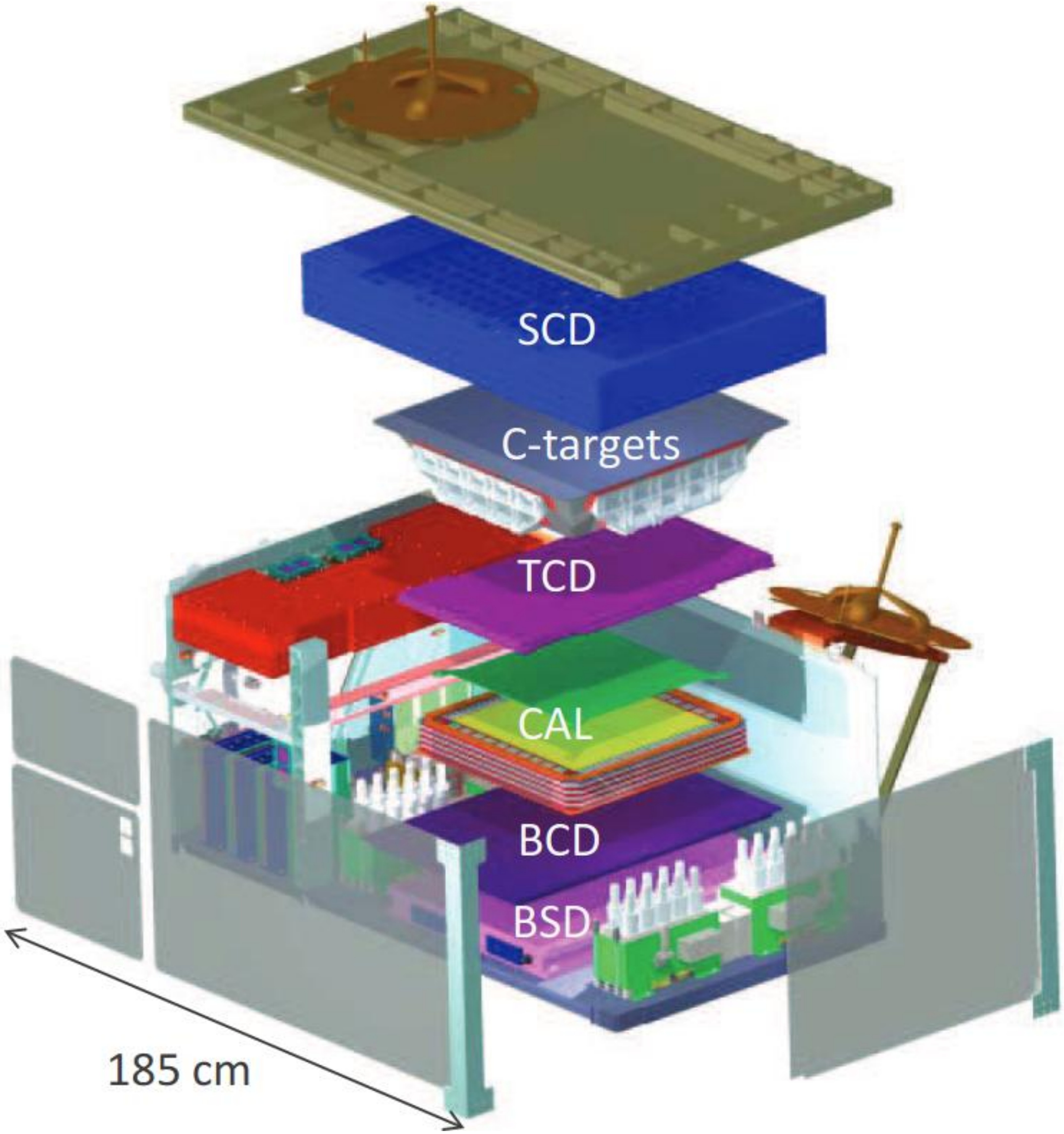

The NUCLEON apparatus

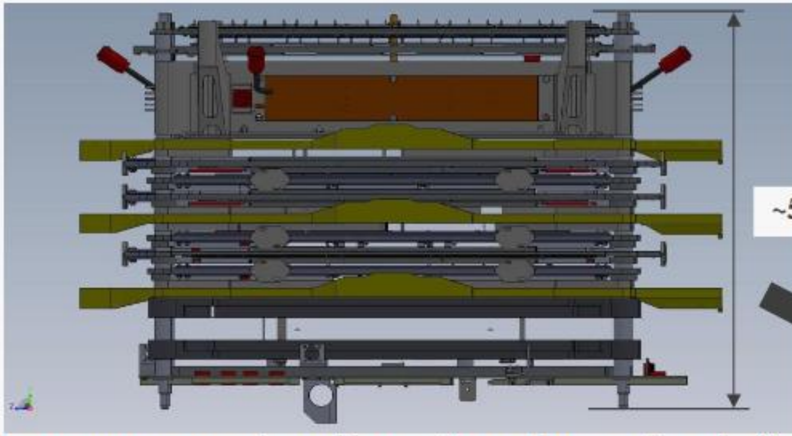

- **Charge measurement system** – four planes of pad silicon detectors (1.5×1.5 cm^2) (**1**);
- **tracker for KLEM energy measurement** – carbon target of 0.25 proton interaction lengths (**2**) and six planes of microstrip silicon detectors (0.4mm pitch) with tungsten between them (~2mm each, ~3 X-lengths in total) (**3**);
- **trigger sysytem** – three double scintillator planes (**4**).

Active area 500*500 mm^2.
Geometrical factor ~0.2 m^{2}sr.

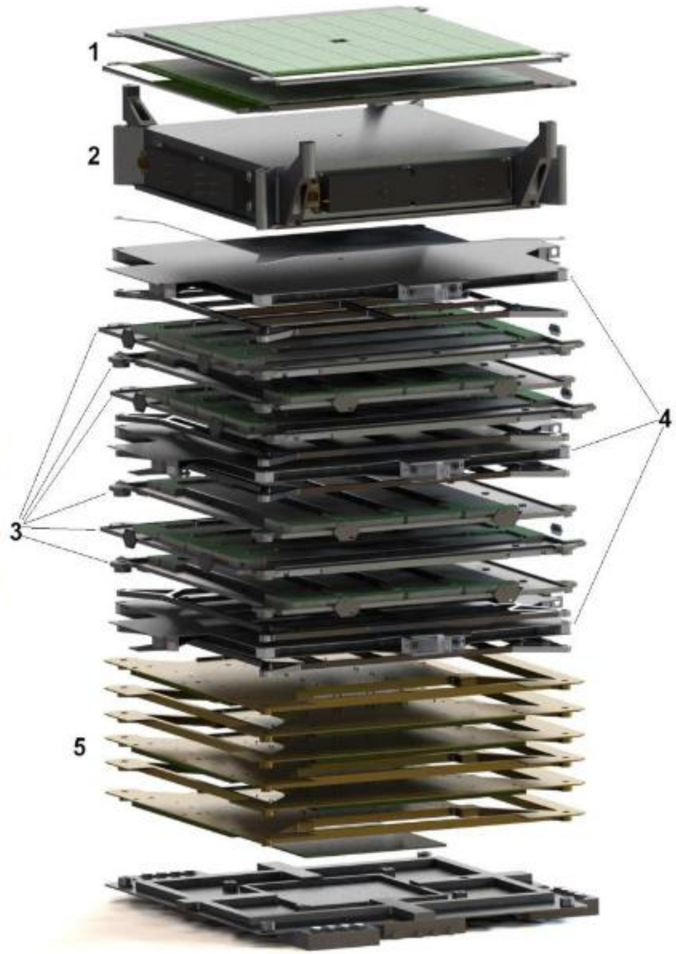

Ionization calorimeter (IC) (**5**) – six planes of tungsten absorber (~8mm each, ~12 X-lengths in total) with silicon strip detectors (1mm pitch).

Active area 250*250mm^2.
Geometrical factor (together with charge and KLEM systems) ~0.06 m^{2}sr. ~0.2 m^2 sr for nuclei

10604 independent electronic channels in total

Hadrons in the CALET calorimeter

Flight data He candidate with 400 GeV total deposit in instrument

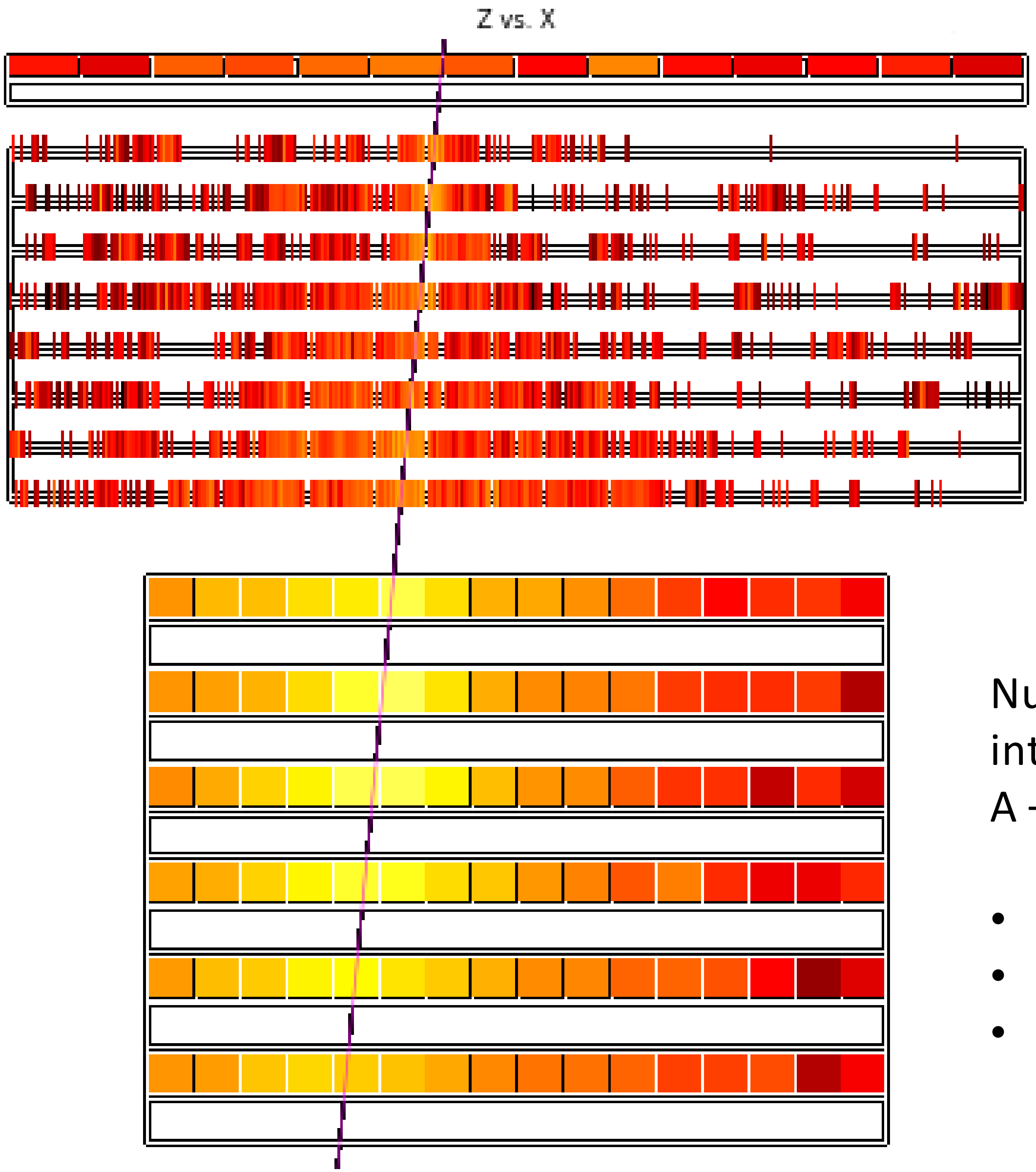

Nuclear interaction:
A + X →

- p, n, A’
- $K^{\pm}$, K^0, $\pi^{\pm} \rightarrow \mu^{\pm}$
- $\pi^0 \rightarrow \gamma\gamma$

Hadron analysis in CALET

Careful validation of selection parameters is performed based on identical analysis in multiple simulation packages:

- EPICS/COSMOS
- Fluka
- Geant4

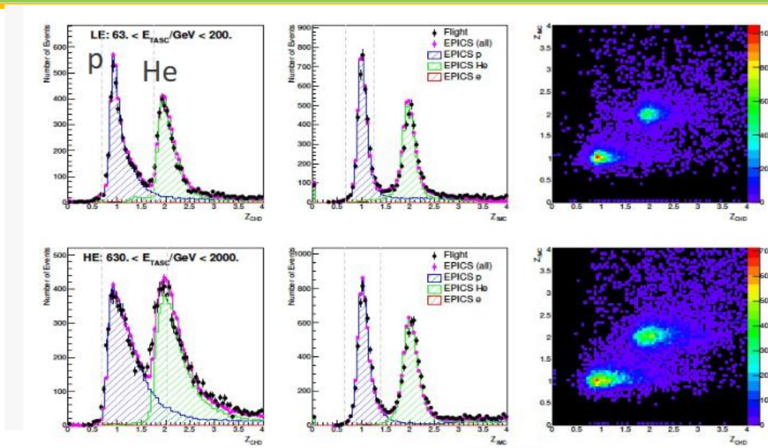

Incomplete list of cuts used:

- Charge selection in CHD
- Combinatorial Kalman Filter tracking
- Require **low** IMC concentration
- Consistency of TASC energy deposits with IMC reconstructed track
- TASC shower topology cuts to remove mis-reconstructed tracks

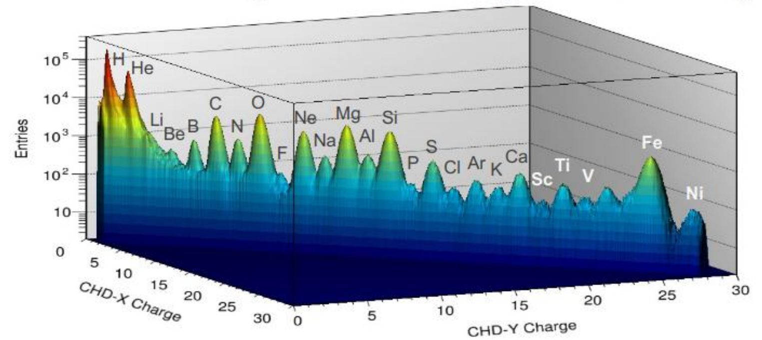

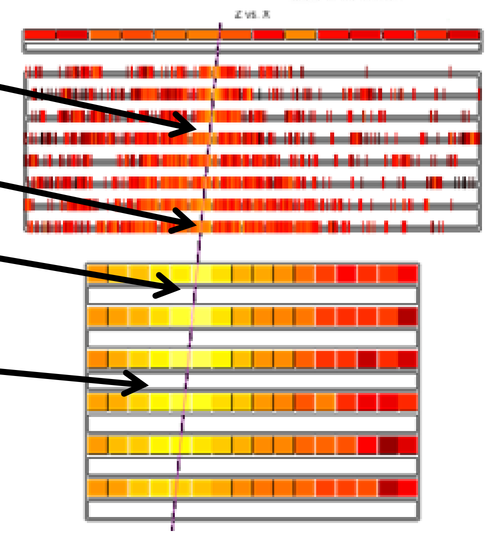

Energy spectrum unfolding

Due to penetrating nature of many secondaries from nuclear interactions, much of the shower energy is carried out of CALET

Primary energy reconstruction is not possible with high precision, but energy spectra can be *unfolded* using iterative Bayesian procedure

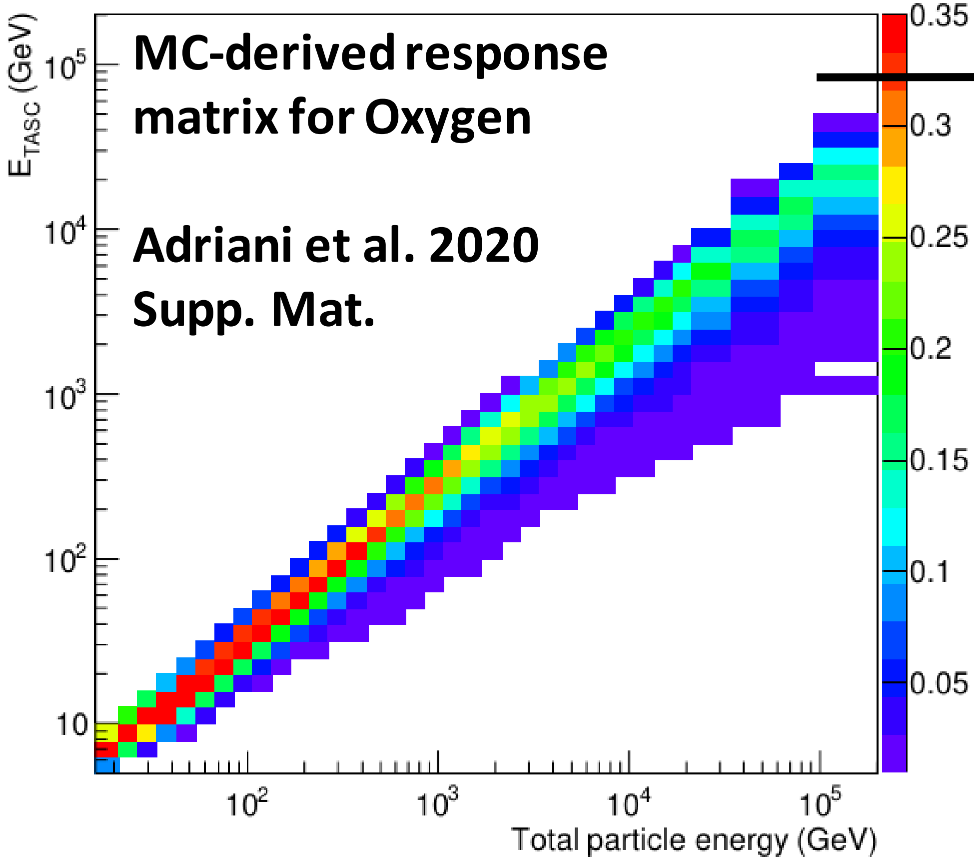

$P(\Delta E \mid E)$: directly from simulations: probability of a given primary energy yielding a given energy deposit in the TASC

$P_0(E)$: input spectrum (model)

$P(E \mid \Delta E)$: obtain from $P(\Delta E \mid E)$ and $P_0(E)$ via Bayes' Theorem

$n(\Delta E)$: observed events with given energy deposit

$P(E)$: "unfolded distribution"

Proton spectrum measurement

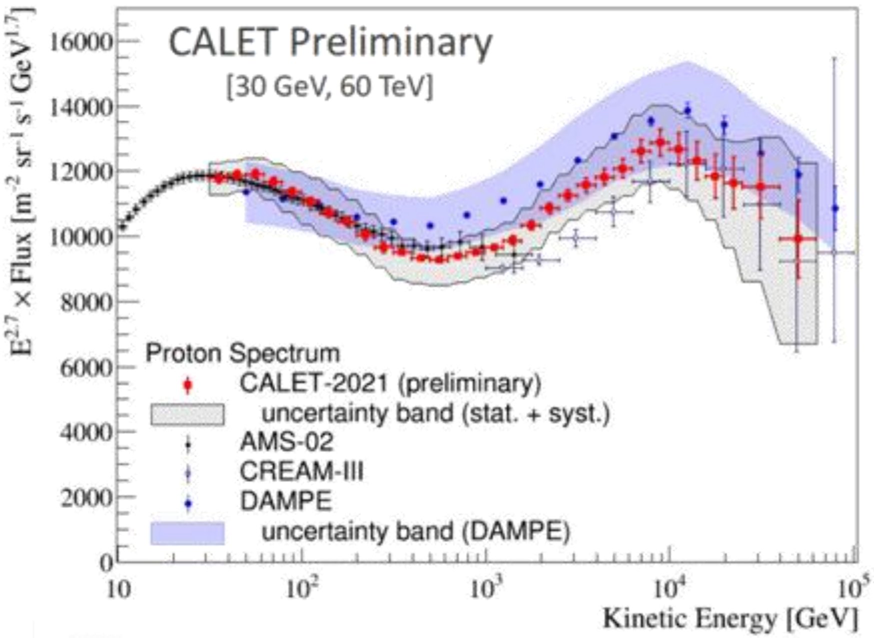

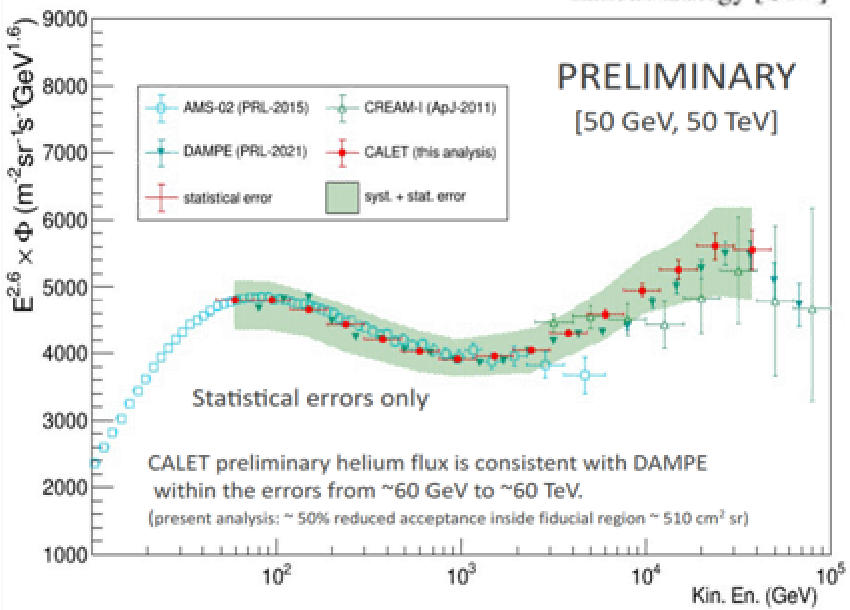

Protons

- Spectral hardening first reported by PAMELA
- CREAM-III reported hard spectrum at TeV energies
- AMS-02 confirmed spectral hardening
- CALET measures over full soft-to-hard transition
- DAMPE extends this to see clear softening
- Preliminary CALET updates show softening as well

Helium

- Spectral hardening also reported by PAMELA
- CREAM-I reported less prominent hardening than protons at TeV energies
- AMS-02 confirmed spectral hardening
- DAMPE measurement demonstrates spectral shape similar to protons
- CALET preliminary results confirm this

Nuclear spectra through Fe

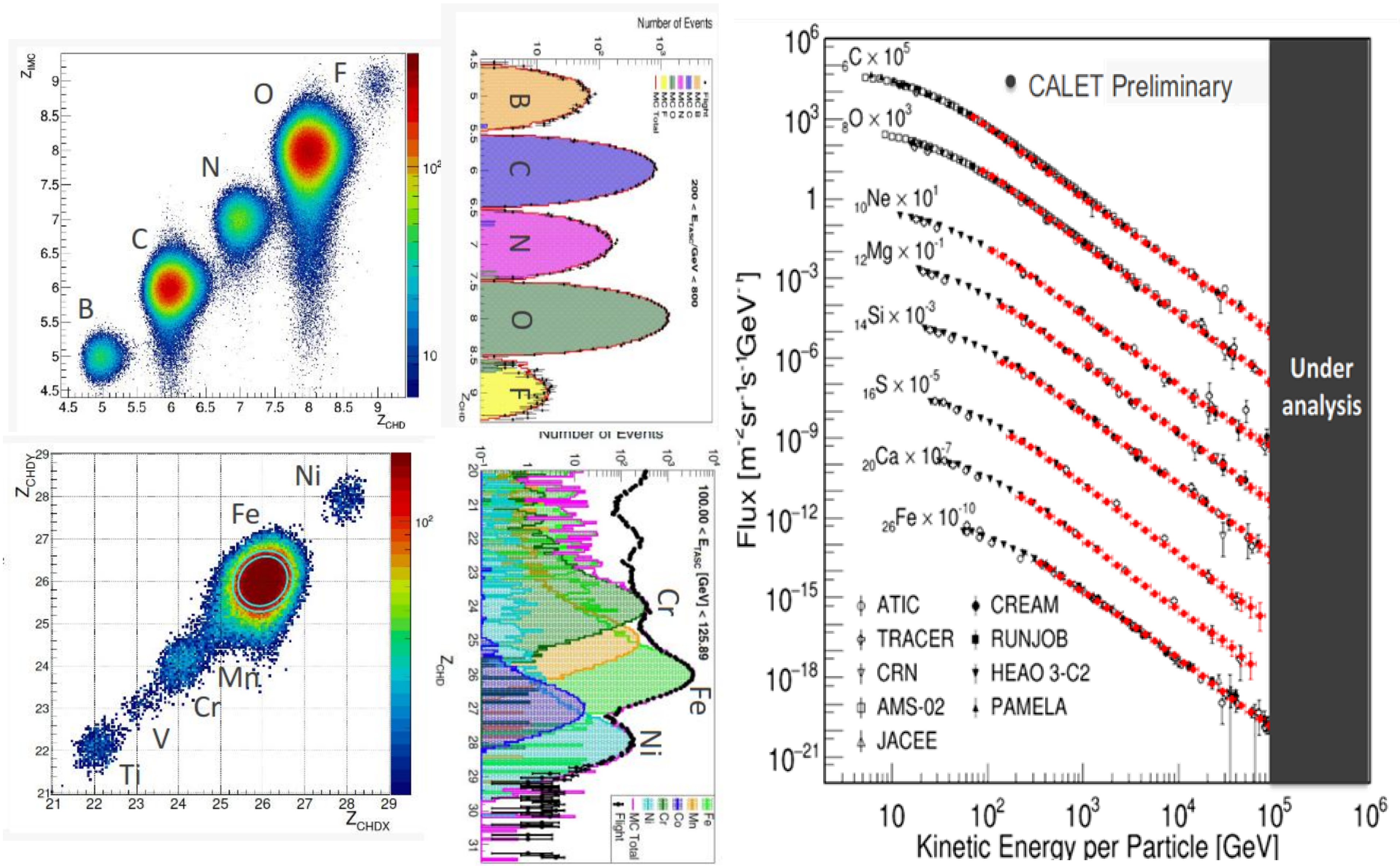

Carbon and Oxygen and C/O ratio

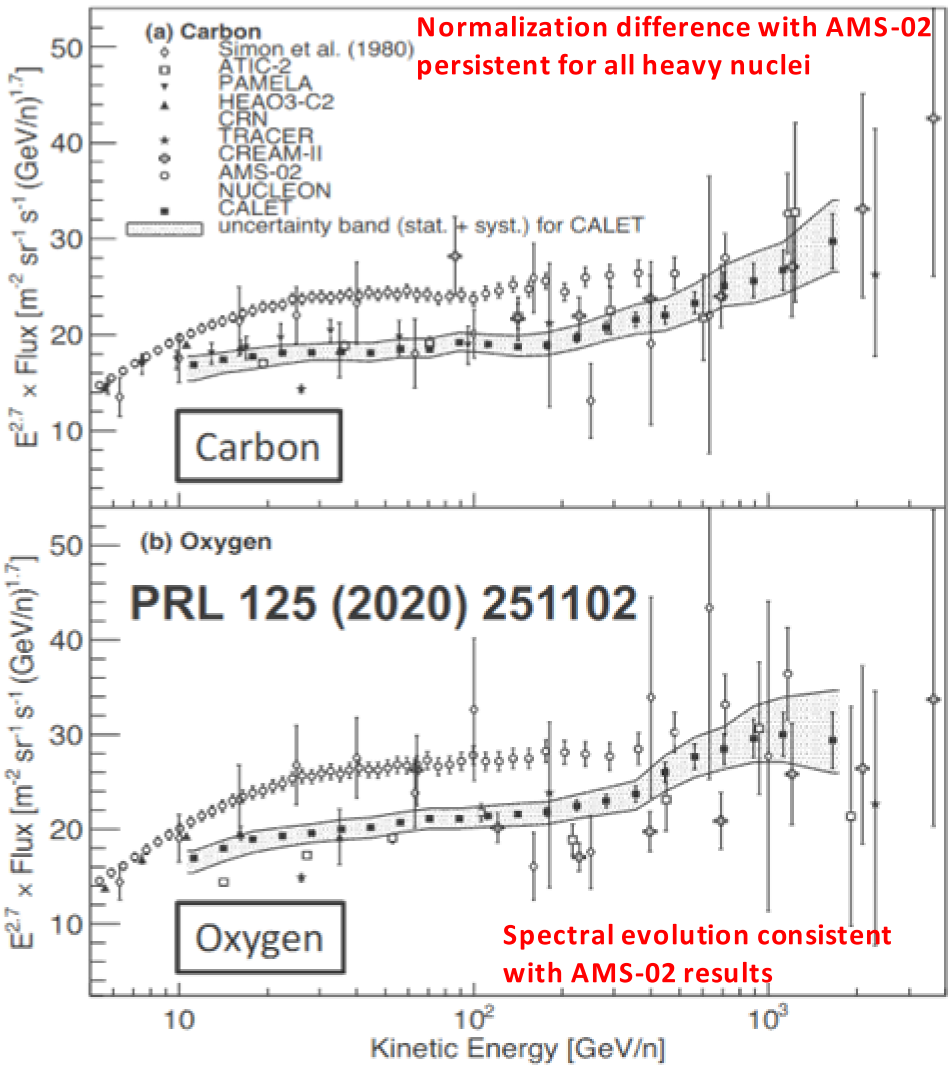

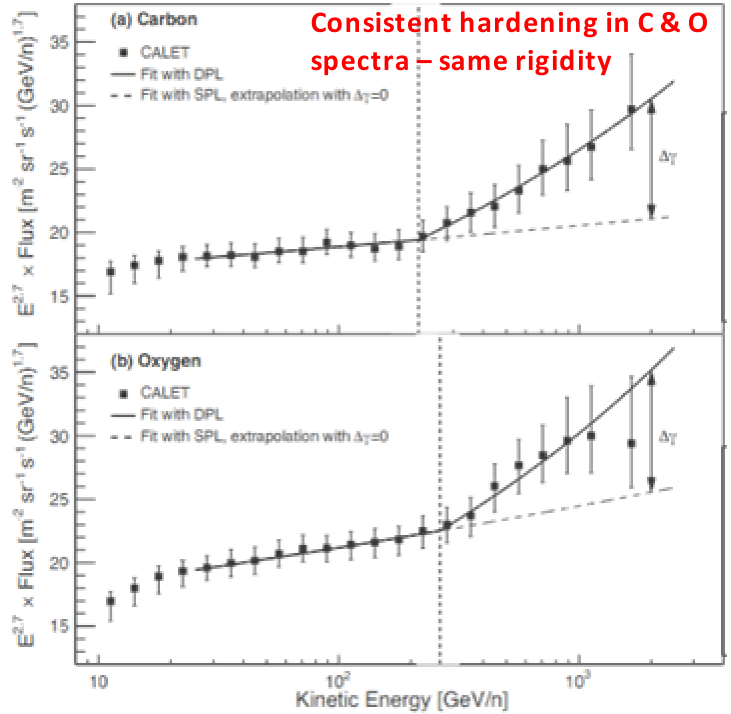

DPL fit: Carbon
$\gamma = -2.663 \pm 0.014$
$E_0 = (215 \pm 54)$ GeV/n
$\Delta\gamma = 0.166 \pm 0.042$
χ^2/dof = 9.0/8

DPL fit: Oxygen
$\gamma = -2.637 \pm 0.009$
$E_0 = (264 \pm 53)$ GeV/n
$\Delta\gamma = 0.158 \pm 0.053$
χ^2/dof = 3.0/8

Carbon and Oxygen and C/O ratio

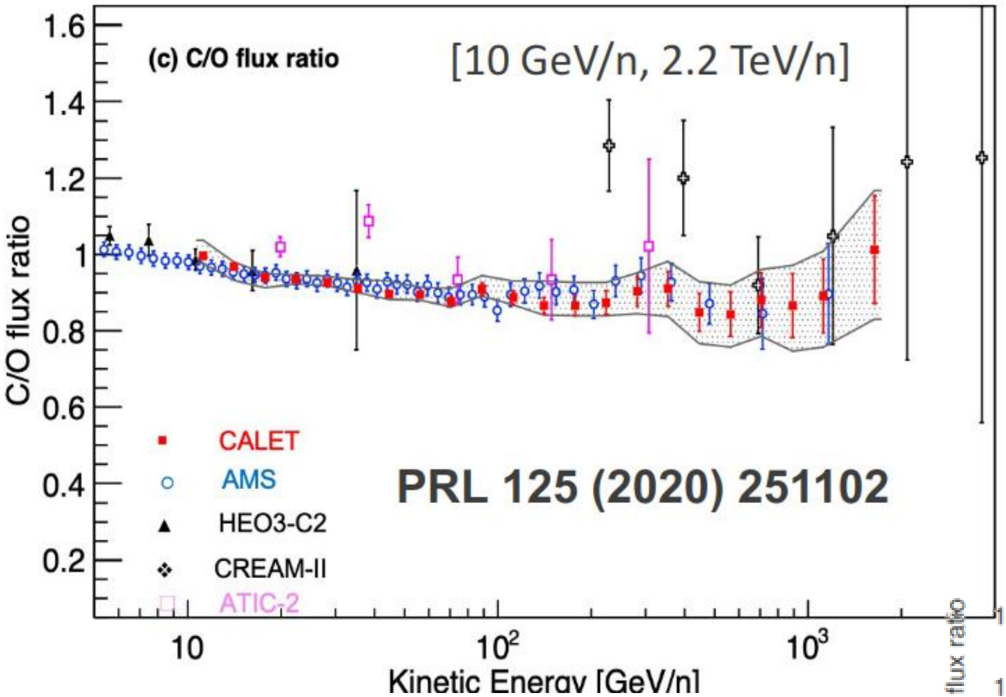

Ratio flat above 25 GeV/nuc
→ same acceleration and propagation history for C and O

(makes sense as both dominant primary)

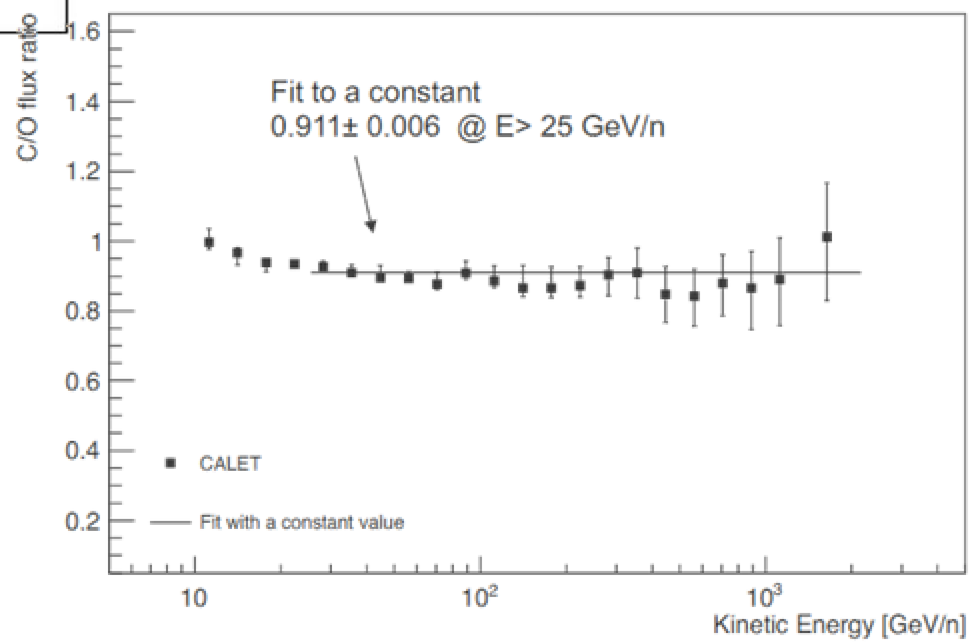

Preliminary Boron-to-Carbon ratio

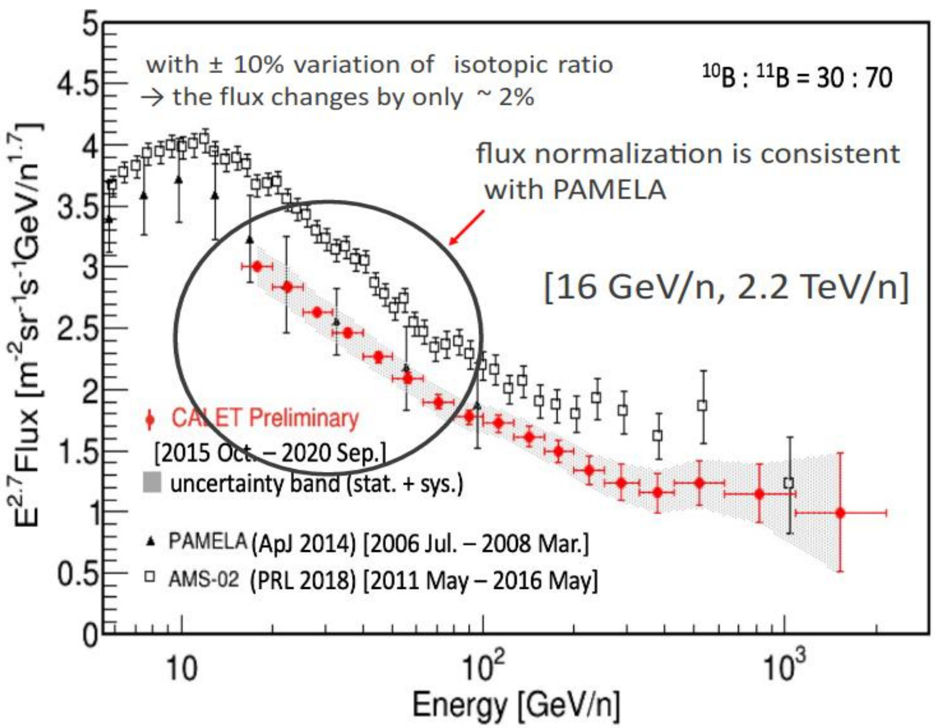

E$^{-1/3}$ dependence

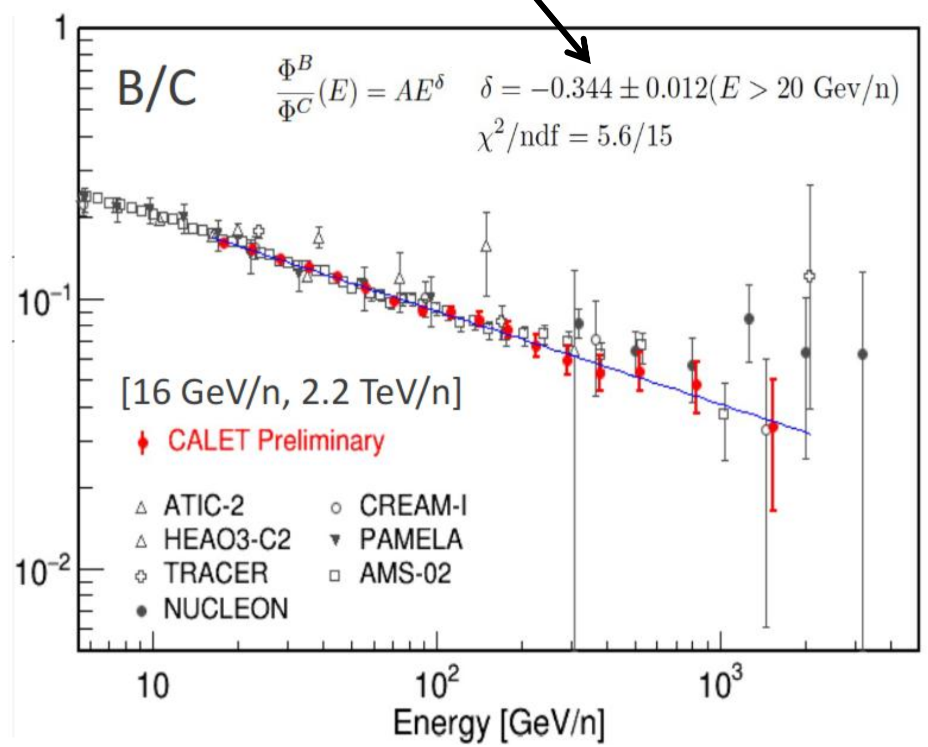

Iron and Nickel and Ni/Fe ratio

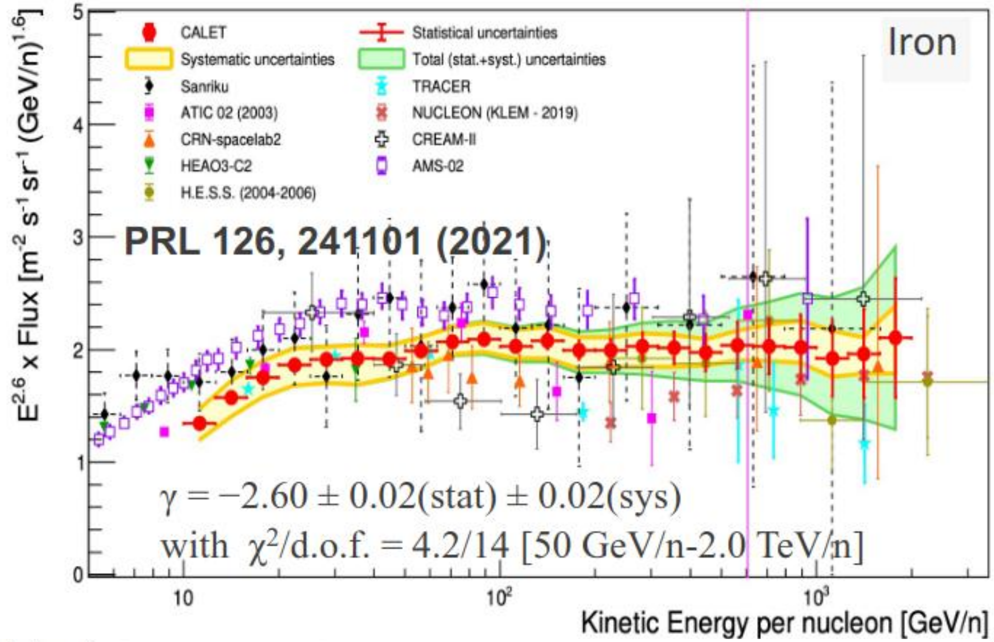

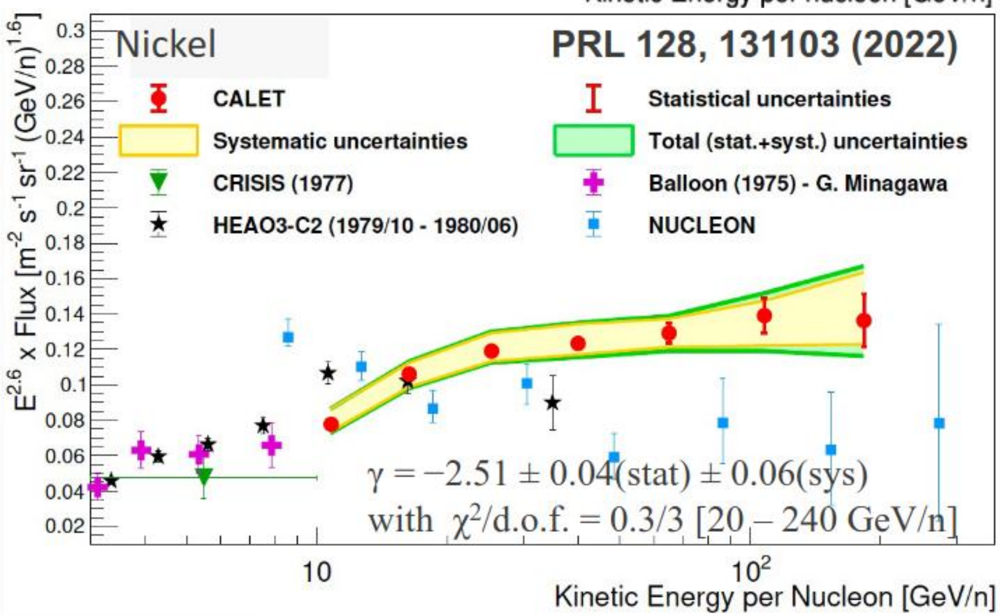

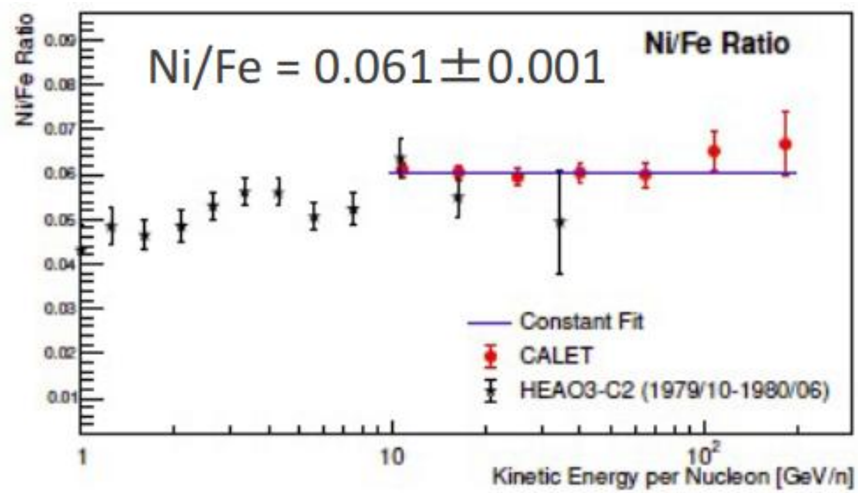

Primary and secondary spectral shapes with AMS-02

L. Derome
EPS-HEP 2019

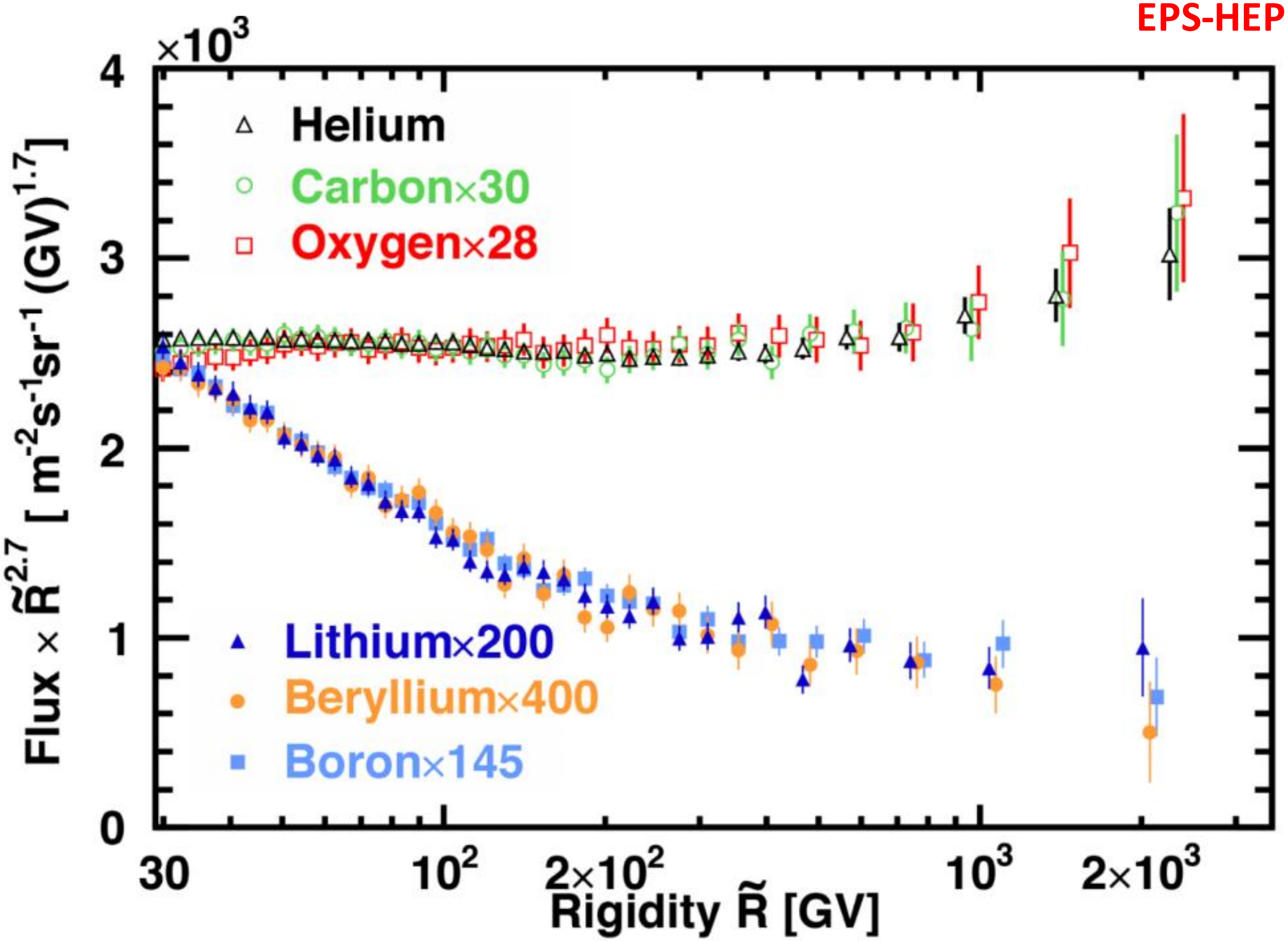

Primary and secondary spectral shapes with AMS-02

Aguilar et al. 2021
PRL 126, 041104

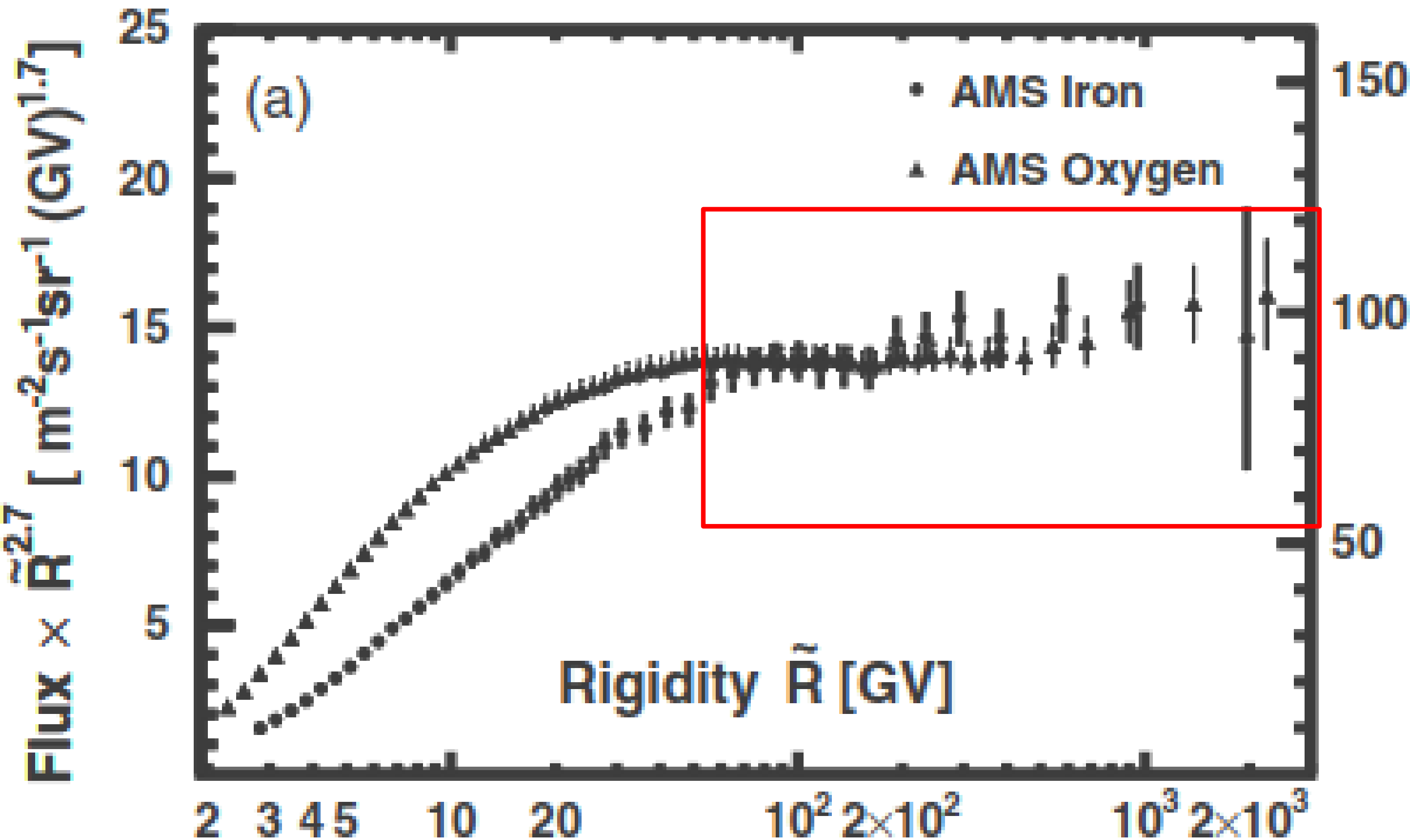

What’s coming next?

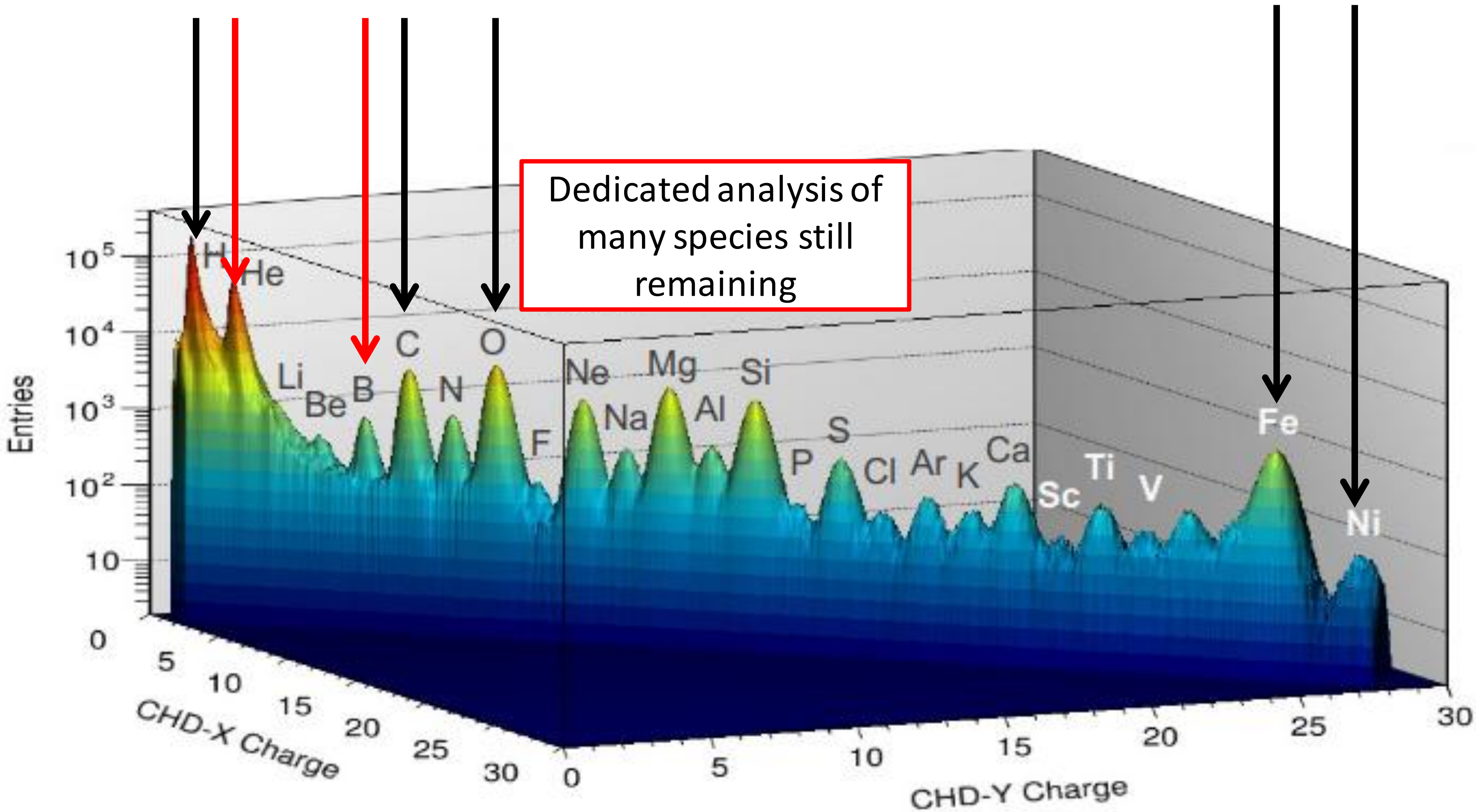

Summary

Element-resolved measurements of GCRs support OB association origins

→ Separation of elements based on T_C when normalized 81% SS + 19% MSM

→ Dividing temperature ~1250K consistent with OB associations

→ Enrichment abundances of MSM from Wolf-Rayet winds and SNe

→ Grain acceleration as injection mechanism favored by refractory enhancement

→ Pattern across elements follows $Z^{2/3}$ grain sputtering cross section

Direct measurements of GCRs push towards the knee

→ Magnetic spectrometers: PAMELA, AMS-02 (, ALADINO?, AMS-100?)

→ Electromagnetic calorimeters: Fermi LAT, NUCLEON, CALET, DAMPE, ISS-CREAM?(, HERD)

→ Abundance measurements: CALET, DAMPE, SuperTIGER(, TIGERISS?)

Primary GCRs ($Z > 1$) show a consistent hardening at comparable rigidities

→ He (and p?) indicates subsequent softening

→ AMS-02 demonstrates hardening in secondaries as well at lower R

→ Cause not resolved- GCR reacceleration? source classes?